AGU100 ADVANCING EARTH AND SPACE SCIENCE

JGR

Journal of Geophysical Research: Earth Surface

RESEARCH ARTICLE
10.1029/2017JF004304

Special Section:
The Arctic: An AGU Joint Special Collection

Six Decades of Glacial Mass Loss in the Canadian Arctic Archipelago

Brice Noël[1], **Willem Jan van de Berg**[1], **Stef Lhermitte**[2], **Bert Wouters**[1], **Nicole Schaffer**[3,4], **and Michiel R. van den Broeke**[1]

[1]Institute for Marine and Atmospheric Research Utrecht, Utrecht University, Utrecht, Netherlands, [2]Department of Geoscience and Remote Sensing, Delft University of Technology, Delft, Netherlands, [3]Department of Geography, Environment and Geomatics, University of Ottawa, Ottawa, Ontario, Canada, [4]Centro de Estudios Avanzados en Zonas Áridas (CEAZA), Universidad de La Serena, La Serena, Chile

Key Points:
- The Canadian Arctic Archipelago experienced six decades of glacial mass loss
- Predominant negative NAO conditions in the last two decades significantly warmed the near-surface climate, accelerating the mass loss
- NCAA ice caps compensate enhanced melt through active refreezing in firn, whereas SCAA ice fields lost most of their buffering capacity

Supporting Information:
- Supporting Information S1

Correspondence to:
B. Noël,
b.p.y.noel@uu.nl

Citation:
Noël, B., van de Berg, W. J., Lhermitte, S., Wouters, B., Schaffer, N., & van den Broeke, M. R. (2018). Six decades of glacial mass loss in the Canadian Arctic Archipelago. *Journal of Geophysical Research: Earth Surface*, *123*, 1430–1449. https://doi.org/10.1029/2017JF004304

Received 30 MAR 2017
Accepted 12 MAY 2018
Accepted article online 23 MAY 2018
Published online 22 JUN 2018

Abstract The Canadian Arctic Archipelago comprises multiple small glaciers and ice caps, mostly concentrated on Ellesmere and Baffin Islands in the northern (NCAA, Northern Canadian Arctic Archipelago) and southern parts (SCAA, Southern Canadian Arctic Archipelago) of the archipelago, respectively. Because these glaciers are small and show complex geometries, current regional climate models, using 5- to 20-km horizontal resolution, do not properly resolve surface mass balance patterns. Here we present a 58-year (1958–2015) reconstruction of daily surface mass balance of the Canadian Arctic Archipelago, statistically downscaled to 1 km from the output of the regional climate model RACMO2.3 at 11 km. By correcting for biases in elevation and ice albedo, the downscaling method significantly improves runoff estimates over narrow outlet glaciers and isolated ice fields. Since the last two decades, NCAA and SCAA glaciers have experienced warmer conditions (+1.1°C) resulting in continued mass loss of 28.2 ± 11.5 and 22.0 ± 4.5 Gt/year, respectively, more than doubling (11.9 Gt/year) and doubling (11.9 Gt/year) the pre-1996 average. While the interior of NCAA ice caps can still buffer most of the additional melt, the lack of a perennial firn area over low-lying SCAA glaciers has caused uninterrupted mass loss since the 1980s. In the absence of significant refreezing capacity, this indicates inevitable disappearance of these highly sensitive glaciers.

Plain Language Summary Outside the ice sheets of Greenland and Antarctica, the Canadian Arctic Archipelago is home to 14% of the world's ice-covered area. Ice caps can be found on Ellesmere and Baffin Islands in the north and south of the archipelago. Here we present a novel daily, 1 km surface mass balance product for the period 1958–2015 that allows us to quantify the contemporary mass loss of Canadian ice caps and identify the acting processes. The high-resolution product realistically resolves local patterns of mass change over narrow glaciers and confined ice fields that are often found in the Canadian Arctic. We show that these ice caps have been losing mass for decades and that mass loss accelerated in 1996. This followed a significant warming (+1.1°C), which increased the production of meltwater. While the snow covering the interior of the northern ice caps can still buffer most of this additional melt through refreezing, the lack of a perennial snow cover over low-lying southern ice caps caused uninterrupted mass loss since the 1980s. If this trend is not reversed, these southern ice caps might disappear within 400 years.

1. Introduction

The Canadian Arctic Archipelago (CAA) is home to one of the world's largest glaciated areas (~148,000 km^2), comprising ~14% of Earth's total ice-covered area outside the ice sheets of Greenland and Antarctica (Sharp et al., 2011a). Most glaciers and ice caps can be found on Ellesmere, Devon, Axel Heiberg, and Meighen Islands forming the northern archipelago (Northern Canadian Arctic Archipelago [NCAA]; ~106,000 km^2) and on Baffin-Bylot Islands located further south (Southern Canadian Arctic Archipelago [SCAA]; ~42,000 km^2; see inset in Figure 1). The NCAA encompasses small ice caps feeding marine-terminating glaciers and flowing into narrow fjords. Van Wychen et al. (2016) estimated the NCAA glacial discharge at 2.2 ± 0.7 Gt/year, with small temporal variability. In a recent study, Millan et al. (2017) showed that NCAA ice discharge decreased from 4.5 ± 0.5 Gt/year in 1991 to 3.5 ± 0.5 Gt/year in 2000, with no significant change afterward.

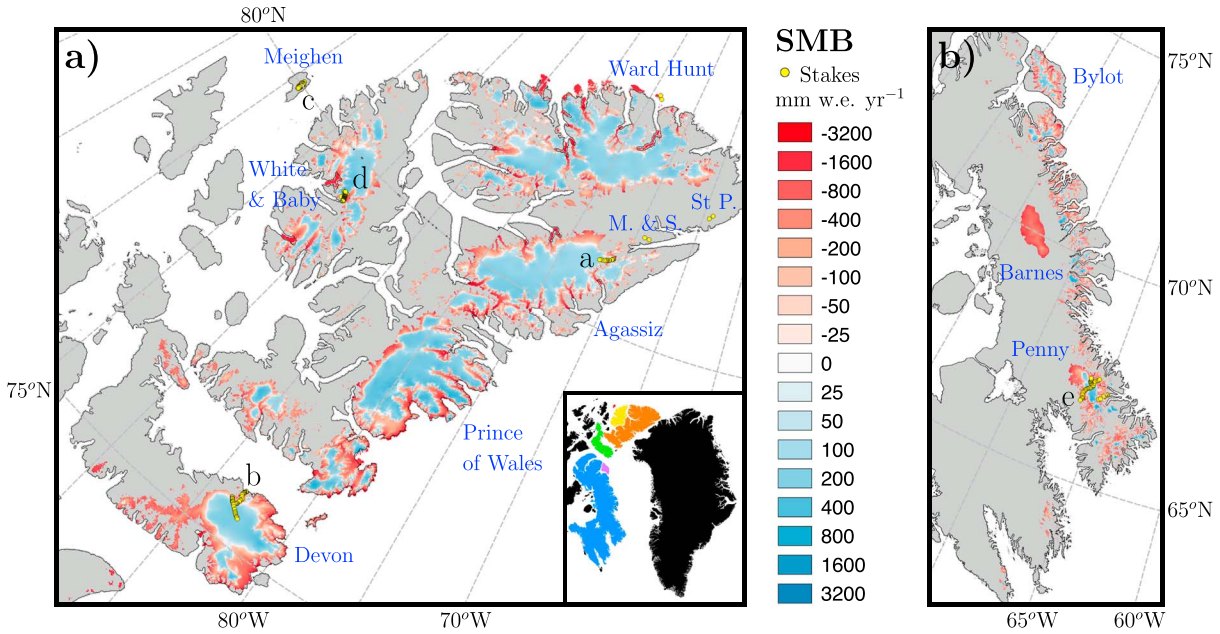

Figure 1. Average SMB of (a) NCAA and (b) SCAA for the period 1958–2015. SMB observations used for evaluation and calibration are displayed as yellow dots. Letters refer to the five transects showed in Figures S3a–S3e. The maps show the location and name of NCAA and SCAA ice caps. The inset locates the ice-covered CAA islands relative to Greenland: Ellesmere (orange), Axel Heiberg (yellow), Meighen (red), Devon (green), Baffin (blue), and Bylot (purple). NCAA = Northern Canadian Arctic Archipelago; SCAA = Southern Canadian Arctic Archipelago; SMB = surface mass balance; CAA = Canadian Arctic Archipelago.

In contrast, the SCAA includes Bylot, Barnes, and Penny ice caps that are flanked by a network of small ice fields and disconnected grounded glaciers, contributing little to glacial discharge (~0.06 Gt/year; Van Wychen et al., 2015).

Recent satellite gravimetry Gravity Recovery and Climate Experiment (GRACE) and altimetry Ice, Cloud and land Elevation Satellite (ICESat) measurements (Gardner et al., 2013) revealed that over the period 2003–2009 NCAA and SCAA lost mass at a rate of 33 ± 4 and 27 ± 4 Gt/year, respectively. Under a moderate warming scenario (Representative Concentration Pathways (RCP) 4.5), CAA glaciers could lose ~18% of their volume by the end of the 21st century, yielding 0.35 ± 0.24 mm/year of sea level rise (Lenaerts et al., 2013).

To date, the horizontal resolution used in regional climate models, typically 5 to 20 km, remains insufficient to accurately resolve the complex topography of the CAA's small ice bodies. As a consequence, modeled surface mass balance (SMB) components, notably surface melt and runoff, are affected by significant biases in elevation, hypsometry, and ice albedo (Noël et al., 2016, 2017). Lenaerts et al. (2013) evaluated the output of the regional climate model RACMO2.1 at 11 km (1960–2011) against point SMB and near-surface temperature measurements collected in the NCAA (Gardner et al., 2011). SMB components were corrected for a hypsometry bias, that is, an overestimation of glacierized area below 1,000 m in the RACMO2.1 ice mask. The remaining discrepancies were attributed to model elevation bias and local meteorological processes unresolved in RACMO2.1 (Lenaerts et al., 2013). In addition, a direct comparison between mass loss retrieved from GRACE and estimated from combined solid ice discharge data and modeled SMB showed generally good agreement (Lenaerts et al., 2013). Gardner et al. (2011) used a positive degree-days (PDD) SMB model presented in Gardner and Sharp (2009) to reconstruct daily NCAA SMB for the period 1949–2009 at a resolution of 500 m. The PDD model was forced by the National Center for Environmental Prediction/National Center for Atmospheric Research Reanalysis 1. The PDD model was bias corrected using lapse rate estimates derived from local precipitation and temperature measurements. The PDD model successfully reproduced the recent mass loss in NCAA, but the paucity of in situ observations precluded estimation of contemporary SMB changes in SCAA (Gardner et al., 2011).

Here we present a daily, 1 km data set of SMB components covering both NCAA and SCAA for the period 1958–2015 (Figure 1). RACMO2.3 SMB components are statistically downscaled from the original model resolution of 11 km to 1 km. The downscaling procedure corrects for biases in elevation and ice albedo using a digital elevation model (DEM), glacier outlines, and ice albedo product at 1 km resolution. The method resolves all SMB components, that is, total precipitation (PR), total melt (ME), runoff (RU), refreezing (RF),

sublimation (SU), and drifting snow erosion (ER), at high spatial (1 km) and temporal (daily) resolution. Previously, it has been successfully applied to the Greenland ice sheet and surrounding glaciers and ice caps (Noël et al., 2016, 2017).

Section 2 briefly describes the regional climate model RACMO2.3, the 1 km DEM, glacier outlines and ice albedo products used to downscale the SMB components, and in situ SMB measurements used for evaluation. The downscaling procedure, product evaluation, and resulting uncertainties are discussed in section 3. Sections 4 and 5 describe the contemporary climate of CAA glaciers and the recent changes. A more detailed analysis of mass loss acceleration over one NCAA and the three major SCAA ice caps is provided in section 6. Section 7 discusses the remaining limitations of the downscaling procedure, followed by conclusions in section 8.

2. Model and Data

Methods closely follow Noël et al. (2016, 2017), who applied the downscaling technique to the Greenland ice sheet and peripheral glaciers and ice caps.

2.1. The Regional Climate Model RACMO2.3

The Regional Atmospheric Climate Model (RACMO2.3; Van Meijgaard et al., 2008; Noël et al., 2015) combines the physics and dynamics from the European Center for Medium-Range Weather Forecasts-Integrated Forecast System (White, 2001) and the High Resolution Limited Area Model (Undèn et al., 2002). To simulate the climate of polar regions, RACMO2.3 incorporates a multilevel snow module, accounting for melt, runoff, percolation, and refreezing (Ettema et al., 2010). The model also includes a prognostic snow grain size albedo scheme (Munneke Kuipers et al., 2011) and a routine calculating drifting snow sublimation and erosion (Lenaerts et al., 2012). In this study, RACMO2.3 is forced by 6-hourly data from ERA-40 (1958–1978; Uppala et al., 2005) and ERA-Interim reanalyses (1979–2015; Dee et al., 2011). The integration domain includes Greenland, Svalbard, Iceland, and the Canadian Arctic at a horizontal resolution of 11 km. Topography and ice mask of the Canadian Arctic are derived from the GTOPO30 data set at 30'' (Gesch & Larson, 1998) and the Global Land Cover Characteristics (European Center for Medium-Range Weather Forecasts-Integrated Forecast System, 2008) at 1 km resolution, respectively. Bare ice albedo is prescribed from MODerate-resolution Imaging Spectroradiometer (MODIS) surface albedo, averaged for the period 2001–2010 (Noël et al., 2015; Van Angelen et al., 2012).

2.2. DEM, Glacier Outlines, and Ice Albedo

The downscaling method uses high-resolution fields of elevation, ice mask, and ice albedo to correct for RACMO2.3 biases. CAA topography and glacier outlines are downsampled to 1 km using the Canadian Digital Elevation Model (CDEM; Government of Canada Natural Resources Canada Map Information Branch, 2016) at 0.75'' (~20 m; Figure S1a in the supporting information) and the Randolph Glacier Inventory 5.0 (Pfeffer et al., 2014). Bare ice albedo is obtained by averaging the 5% lowest surface albedo measurements from the 500 m MODIS 16-day albedo product (MCD43A3) for the period 2000–2015. Ice albedo ranges from 0.15 over dark low-lying glaciers to 0.55 for bright ice located under the perennial firn layer in the CAA accumulation zones (Figure S1b).

2.3. In Situ SMB Measurements

For evaluation and calibration, we use 4,356 SMB measurements (yellow dots in Figure 1) collected in NCAA (198 sites; Gardner et al., 2011) and in SCAA (39 sites; N. Schaffer, personal communication, 2016). In NCAA, observations are retrieved from transects on four ice caps, namely, Agassiz, Devon, Meighen, and White glacier (a–d in Figure 1a) and four smaller ice fields, that is, Baby, Murray and Simmons, and St Patrick. All measurements in SCAA are concentrated on Penny ice cap (e in Figure 1b). Measurements span the period 1959–2010 and 2006–2014 in NCAA and SCAA, respectively. Observations from eight sites with a >100 m height difference relative to the 1 km CDEM elevation were rejected.

3. Methods

3.1. Downscaling Procedure

The downscaling method, described in Noël et al. (2016), is applied to CAA glaciers with adjusted settings. Combining elevation and ice albedo corrections, the output of RACMO2.3 is statistically downscaled to 1 km using the topography and glacier outlines from CDEM (Figure S1a) and Randolph Glacier Inventory

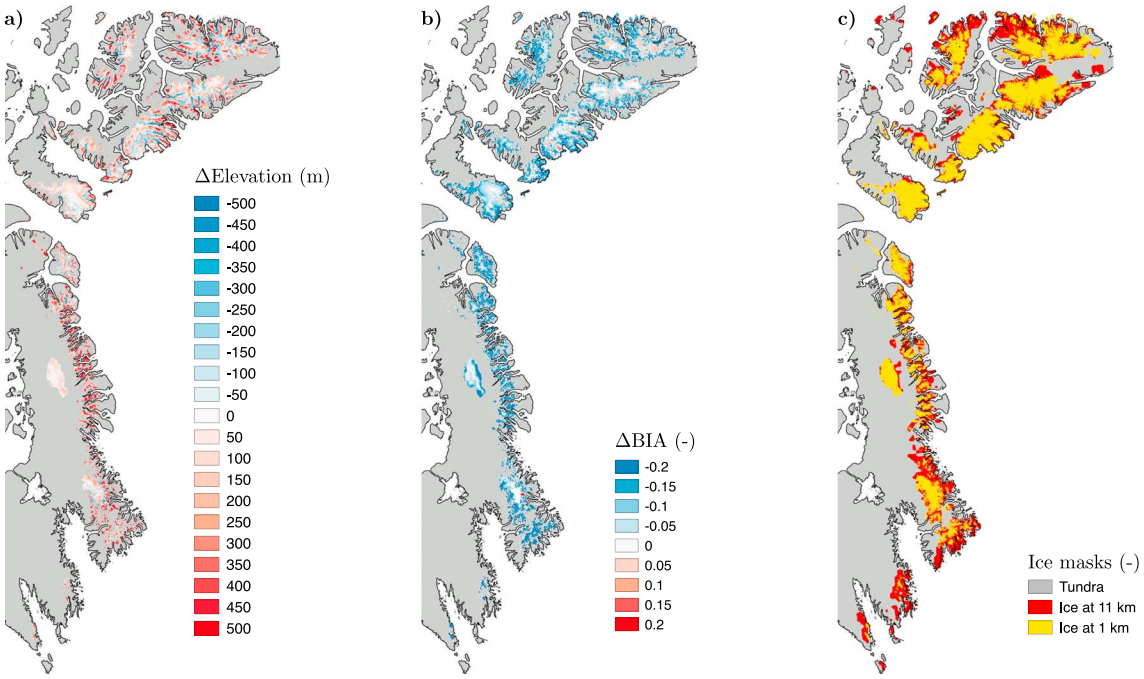

Figure 2. Difference in (a) elevation, (b) bare ice albedo, and (c) ice mask between the 1 km product and RACMO2.3 at 11 km. Negative values represent an overestimation in RACMO2.3. BIA = bare ice albedo; RACMO2.3 = Regional Atmospheric Climate Model version 2.3.

(yellow in Figure 2c) and the 1 km bare ice albedo product from MODIS (Figure S1b). A significant correlation to altitude is essential to correct SMB components for elevation bias, for which runoff (RU), melt (ME), and sublimation qualify (Figures S2a–S2c). Snow drift erosion (ER, not shown) and total precipitation, including solid and liquid precipitation, and snowfall (SF) show no systematic correlation with elevation (Figures S2d and S2e) and are simply bilinearly interpolated to the 1 km glacier outlines, without correcting for elevation. The daily 1 km climatic mass balance (Cogley et al., 2011), hereafter referred to as SMB, is reconstructed as follows:

$$\mathrm{SMB} = \mathrm{PR} - \mathrm{RU} - \mathrm{SU} - \mathrm{ER} \quad (1)$$

Contrary to Noël et al. (2016), no additional correction is applied to total precipitation as no systematic SMB bias relative to in situ measurements could be identified in the accumulation zones, where SMB is primarily governed by precipitation (see section 3.2.1). However, to better partition total precipitation into snowfall and rainfall, we use the fraction of snowfall on total precipitation (SF_{frac}) which shows a strong positive correlation with altitude on ice-covered regions (yellow line in Figure S2f), indicating that solid precipitation prevails in the ice caps' interior. Statistically downscaling SF_{frac} on a daily basis over land ice allows to estimate corrected snowfall and calculate rainfall (RA) as a residual:

$$\mathrm{SF} = \mathrm{PR} \times \mathrm{SF}_{\mathrm{frac}} \quad (2)$$

$$\mathrm{RA} = \mathrm{PR} \times (1 - \mathrm{SF}_{\mathrm{frac}}) \quad (3)$$

3.1.1. Elevation Correction

To correct for elevation bias in RACMO2.3 (Figure 2a), daily regression parameters between SMB components and the model elevation are estimated for each glacierized grid cell at 11 km resolution. Using at least five adjacent pixels, a local regression slope (b_{11km}; mm w.e./m) is calculated and applied to the current grid cell in order to estimate the SMB component at mean sea level (a_{11km}; mm w.e.). Because CAA glaciers cover a relatively small area and show complex geometries, many ice bodies are not or not well resolved in RACMO2.3 (Figure 2c). To address this issue, regression parameters are extrapolated outward of the 11 km ice mask by averaging b_{11km} from at least three adjacent glaciated pixels. These regression parameters are then bilinearly

interpolated to the 1 km glacier outlines to derive an estimate of b_{1km} and a_{1km}. Using the CDEM topography (h_{1km}), runoff, melt, and sublimation ($X_{v0.2}$) are calculated at 1 km:

$$X_{v0.2} = a_{1km} + b_{1km} \times h_{1\,km} \tag{4}$$

The downscaled data set that only uses elevation correction is referred to as version v0.2.

3.1.2. Ice Albedo Correction

The albedo of exposed bare ice is generally overestimated in RACMO2.3 (Figure 2b). Here melt and runoff in v0.2 are adjusted to account for the resulting lack of ice melt (ME_{add}) in dark, low-lying regions.

$$ME_{add} = \Delta\alpha \times 0.5 \times \frac{SW_{dir\,1\,km}}{L_f} \times (1 + \xi) \tag{5}$$

where ME_{add} (mm w.e./day) is the additional amount of ice melt calculated at 1 km, $\Delta\alpha$ (-) is the difference between the averaged bare ice albedo retrieved from the set of regression cells used to downscale runoff at 11 km and the MODIS albedo product at 1 km, $SW_{dir\,1\,km}$ is the modeled daily cumulated downward shortwave radiation bilinearly interpolated to 1 km, and L_f is the latent heat of fusion (3.337×10^5 J/kg^{-1}). To account for the slope of the glacier surface, the dimensionless correction factor for a tilted plane ξ is applied to the direct component of modeled downward shortwave radiation. This correction is required as RACMO2.3 model radiation assuming a horizontal surface. This factor ranges from 0 for north sloping glaciers to values larger than 1 for south oriented slopes.

The ratio $\mathbf{\Gamma}$ between daily downscaled runoff and melt in v0.2 is applied to ME_{add} to calculate the additional runoff (RU_{add}).

$$RU_{add} = \mathbf{\Gamma} \times ME_{add} \tag{6}$$

Assuming that the residual misfit between reconstructed and observed SMB (ΔSMB) for the different CAA ablation sites is attributable to underestimated runoff in narrow ablation zones, RU_{add} is then scaled by a factor f_{scale} (0.200), obtained by computing a least squares fit minimizing ΔSMB using both NCAA and SCAA ablation measurements. The fact that f_{scale} is much smaller than 1 suggests that the elevation bias in RACMO2.3 is the dominant factor contributing to ΔSMB and that the ice albedo correction only slightly further improves the performance of the downscaled product (see section 3.2.1). The low value is also attributed to limitations in the input data as well as in the downscaling procedure (see section 7).

$$f_{scale} = \frac{\sum \Delta SMB \times RU_{add}}{\sum (RU_{add})^2} \tag{7}$$

The adjusted amount of runoff ($RU_{v1.0}$) is obtained by adding RU_{add} to the downscaled runoff ($RU_{v0.2}$):

$$RU_{v1.0} = RU_{v0.2} + f_{scale} \times RU_{add} \tag{8}$$

The corrected melt ($ME_{v1.0}$) is obtained in a similar fashion:

$$ME_{v1.0} = ME_{v0.2} + ME_{add} \tag{9}$$

Refreezing ($RF_{v1.0}$) is estimated as a residual between adjusted melt, runoff, and rainfall:

$$RF_{v1.0} = RA + ME_{v1.0} - RU_{v1.0} \tag{10}$$

The downscaled product combining both elevation and ice albedo corrections is referred to as version v1.0.

3.2. Evaluation and Uncertainties

3.2.1. In Situ Measurements

Figure 3 compares SMB derived from (a) the original output of RACMO2.3 at 11 km, (b) the downscaled product version v0.2, and (c) the corrected downscaled version v1.0 against 4,356 stake measurements collected in NCAA (blue symbols) and SCAA (orange symbols). While RACMO2.3 performs reasonably well in capturing SMB in the high ablation and accumulation zones (SMB > −2 m w.e. in Figure 3a), SMB is overestimated in low-lying regions by 200 mm w.e. on average and up to 4 m w.e. locally. Figure 3b shows that correcting for elevation bias in RACMO2.3 (Figure 2a) significantly improves the agreement with observations: the mean SMB bias is reduced by almost a factor of 2 and R^2 increases by 0.55. Applying the bare ice albedo bias correction (Figure 2b) further improves the performance as indicated by smaller mean SMB bias (40 mm w.e.) and RMSE (380 mm w.e.) and a larger R^2 (0.74).

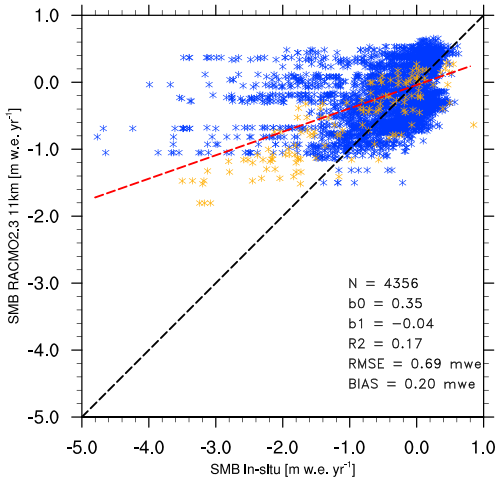

(a) Modelled SMB at 11 km

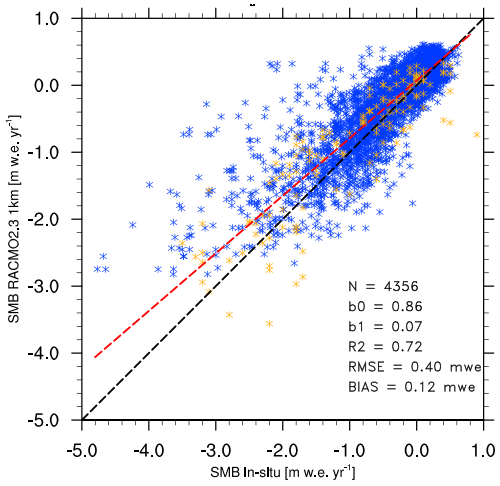

(b) Downscaled SMB at 1 km version v0.2

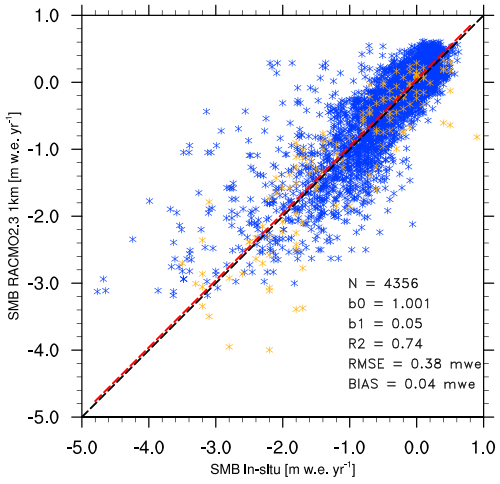

(c) Corrected SMB at 1 km version v1.0

Figure 3. Comparison of SMB observations collected at 237 sites with (a) modeled SMB from RACMO2.3 at 11 km, (b) downscaled SMB at 1 km (v0.2), and (c) corrected downscaled SMB at 1 km (v1.0). The orange symbols correspond to in situ measurements from Penny ice cap (39 sites, SCAA). The red dashed lines represent the regression including all measurements (NCAA and SCAA) using a perpendicular fit. SMB = surface mass balance; RACMO2.3 = Regional Atmospheric Climate Model version 2.3; SCAA = Southern Canadian Arctic Archipelago; NCAA = Northern Canadian Arctic Archipelago.

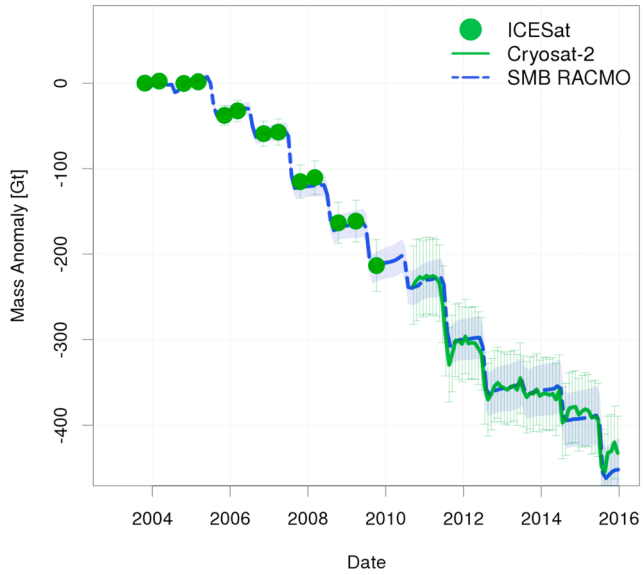

(a) NCAA mass anomaly

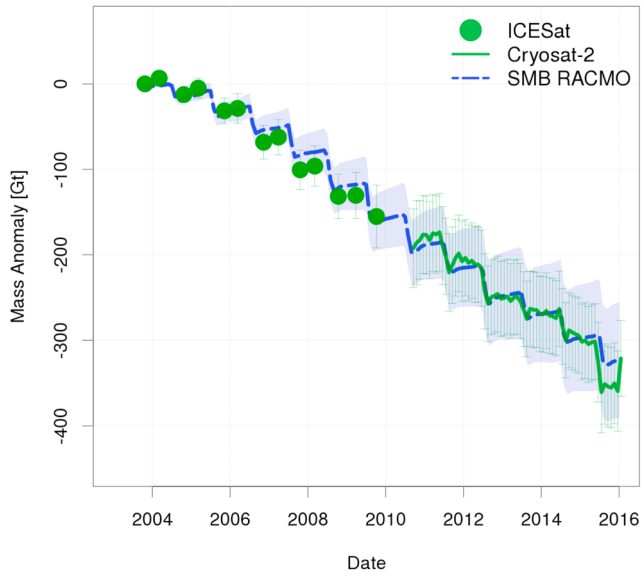

(b) SCAA mass anomaly

Figure 4. Comparison of (a) NCAA- and (b) SCAA-integrated mass anomaly (2004–2015) derived from ICESat (green dots)/CryoSat-2 (green line) altimetry measurements with the downscaled SMB v1.0 (dashed blue line). The light blue envelope represents the estimated uncertainty of the downscaled SMB product. The green bars correspond to estimated uncertainties in ICESat/CryoSat-2 records. NCAA = Northern Canadian Arctic Archipelago; SCAA = Southern Canadian Arctic Archipelago; SMB = surface mass balance; RACMO = Regional Atmospheric Climate Model.

Figures S3a–S3e show observed (red) and downscaled (blue) SMB along five transects (a–e in Figure 1). Agreement is generally good except for low-lying floating glacier tongues of Agassiz, Devon, and Penny ice caps (<300 m; Figures S3a, S3b, and S3e). The reason is that MODIS measures too low surface albedo over floating glacier tongues, as a result of mixing values of adjacent dark melt ponds with brighter dry ice (Noël et al., 2016). Figure S3f shows the progressive performance improvements binned in 0.5 m w.e. SMB intervals. Clearly, the elevation correction in v0.2 dominates the improvements, reducing the RMSE by 53–68% in the ablation zones and by 47% in the accumulation zones, respectively. Relative to v0.2, the ice albedo correction in v1.0 reduces the RMSE by an additional 16% in the low ablation zone (SMB < −2 m w.e.) and by 2–9% at higher elevations.

3.2.2. Product Uncertainty

Following the method outlined in Noël et al. (2017), a product uncertainty of 11.0 and 4.5 Gt/year is obtained for SMB estimates of NCAA and SCAA, respectively. To obtain these, SMB measurements (yellow dots in Figure 1) were binned in 250 mm w.e. intervals for which the mean bias was estimated, that is, modeled minus measured SMB, resulting in 129 mm w.e. for the ablation zones (12 bins) and 162 mm w.e. for the accumulation zones (4 bins). SMB uncertainty is estimated for NCAA and SCAA individually (σ_{XCAA}) by summing the mean ablation bias integrated over their respective ablation zone area (~48,000 and ~32,800 km^2) and the mean accumulation bias over the accumulation area of NCAA and SCAA (~56,400 and ~10,400 km^2).

$$\sigma_{XCAA} = \sqrt{\left(\beta^{abl.} \times A^{abl.}_{XCAA}\right)^2 + \left(\beta^{acc.} \times A^{acc.}_{XCAA}\right)^2} \quad (11)$$

where $\beta^{abl.}$ and $\beta^{acc.}$ are the mean binned bias for the ablation and accumulation zones of CAA, $A^{abl.}_{XCAA}$ is the ablation zone area of NCAA or SCAA, and $A^{acc.}_{XCAA}$ is the accumulation zone area of NCAA or SCAA. The accumulation bias is assumed to be included in the ablation (SMB) bias and therefore not spatially integrated over the ablation zone, as in Noël et al. (2017).

The downscaling technique does not account for hypsometry changes resulting from glacier retreat and volume loss in time. Accounting for these processes (see supporting information), we estimate an additional SMB uncertainty of ~6% in NCAA and 0–2% in SCAA on average for the 1996–2015 period (grey envelope in Figures 5a and 5b and Tables S1 and S2), resulting in an ~4% and 1–5% uncertainty in the recent trends, respectively.

3.2.3. Remote Sensing Records

Elevation changes from ICESat (2003–2009) and CryoSat-2 (2010–2015) measurements were derived following Gardner et al. (2013) and Wouters et al. (2015). For ICESat, observations were grouped every 700 m along repeated ground tracks, whereas for CryoSat-2, neighboring observations are collected within 1 km of each individual echo location. To these clusters of elevation observations, a model is fitted to estimate the local surface topography and elevation rate at the central point, where outliers are removed in an iterative procedure. Local elevation anomalies at the echo locations are estimated by adding the constant elevation rate of a fitted model to the residuals. These anomalies are used to compute monthly volume anomalies for the NCAA and SCAA, respectively. Elevation anomalies are parameterized as a function of absolute elevation using a third-order polynomial. The resulting fit is used to derive regional volume anomalies within 100 m elevation intervals, by multiplying the polynomial value at each interval's midpoint with the total glaciated area within this elevation bin (Moholdt et al., 2010). Finally, volume anomalies are converted to mass anomalies by assuming a constant density profile, using the density of ice below the equilibrium line altitude (ELA) and a density of 600 ± 250 kg/m^3 above the ELA.

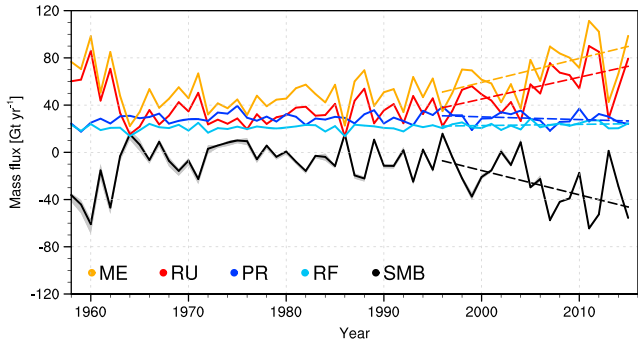

(a) Northern Canadian Arctic Archipelago

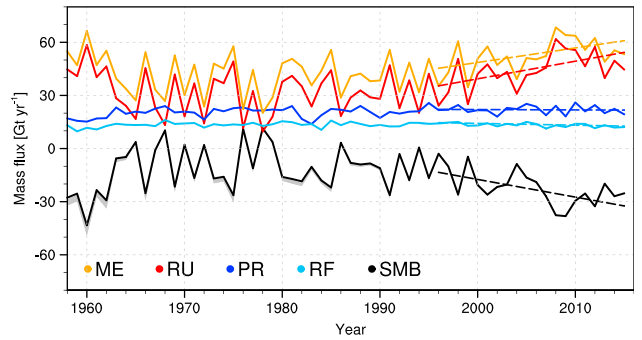

(b) Southern Canadian Arctic Archipelago

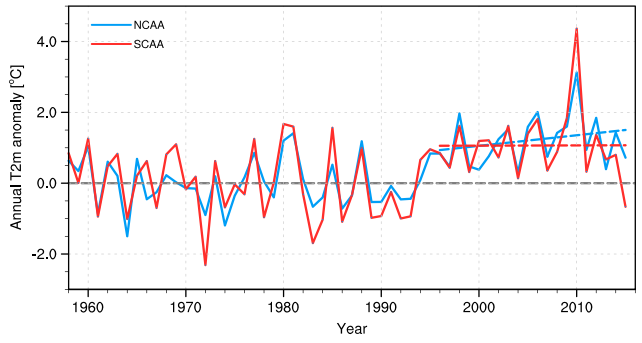

(c) Near-surface temperature anomaly (1958-1995)

Figure 5. Time series of (a) NCAA and (b) SCAA (1958–2015) SMB components: melt (ME), runoff (RU), total precipitation (PR), and refreezing (RF). The grey envelopes correspond to the SMB uncertainty resulting from changing glaciers hypsometry in time, that is, due to glacier retreat and volume loss (see supporting information). Figure 5c shows anomalies in annual mean 2 m temperature for NCAA (blue) and SCAA (red). Anomalies are calculated with respect to the period 1958–1995. Dashed lines show trends for the period 1996–2015. NCAA = Northern Canadian Arctic Archipelago; SCAA = Southern Canadian Arctic Archipelago; SMB = surface mass balance.

Figure 4 further evaluates the SMB product for NCAA and SCAA (dashed blue line) using independently derived mass changes from ICESat and CryoSat-2 altimetry measurements (green dots and line, respectively). The downscaled data set shows excellent agreement with the altimetry records. Both winter accumulation and summer ablation are accurately resolved. In addition, the SMB product falls well within ICESat/CryoSat-2 measurements uncertainty, although mass loss appears underestimated in summer 2015 for SCAA.

Gardner et al. (2011) estimated 2004–2009 mass loss from GRACE to be 39 ± 9 and 24 ± 7 Gt/year for NCAA and SCAA, respectively. The downscaled SMB product shows good agreement with mass loss of 33.8 ± 11.5 Gt/year for the NCAA, that is, the sum of SMB (30.3 ± 11.0 Gt/year) and solid ice discharge (3.5±0.5 Gt/year; Millan et al., 2017) and 24±4.5 Gt/year for the SCAA, assuming negligible discharge (~0.06 Gt/year; Van Wychen et al., 2015). These results are also in line with Gardner et al. (2011), who obtained a 2004–2009 mass loss of −34 ± 13 Gt/year for NCAA, using their PDD SMB model.

4. Contemporary Climate and Recent Changes

Figure 5 shows time series of SMB components (1958–2015) for (a) NCAA, (b) SCAA, and (c) anomalies in annual mean 2 m temperature. Compared to Greenland glaciers and ice caps (Noël et al., 2017), the climate of CAA ice masses is generally warmer and drier, with mean total precipitation of ~340 mm w.e./year. The ice free tundra surrounding the small CAA glaciers (Figure 1) creates warm summer conditions, resulting in high melt rates. In addition, the prevalent northwesterly winds advect dry air to CAA glaciers, resulting in relatively low precipitation (Lenaerts et al., 2013). As a result, summer meltwater production systematically exceeds annual precipitation (Figures 5a and 5b), indicating that refreezing of meltwater plays a key role in sustaining CAA ice masses. While total precipitation shows little temporal variability, meltwater production sharply peaks in warm years (Figure 5c). In the mid-1990s, CAA ice masses experienced a significant near-surface warming (+ 1.1°C), causing enhanced meltwater runoff in both NCAA and SCAA (Figures 5a and 5b).

4.1. Drivers of the Recent Warming

Changes in summer (June-July-August [JJA]) upper atmosphere circulation control the recent CAA warming (Mortimer et al., 2016; Sharp et al., 2011b). Figure 6a shows JJA 700 hPa air temperature from RACMO2 with superimposed wind speed and direction averaged for 1958–1995; changes after year 1996 (1996–2015 minus 1958–1995) are displayed in Figure 6b. For 1958–1995, NCAA and SCAA experience advection of dry and cool polar air in summer (Figure 6a). During the last two decades, anomalously high pressure persisted over Davis Strait along the southwestern coast of Greenland, favoring more frequent northward advection of warmer air by the prevalent westerly winds over the CAA (Figure 6b). This caused successive record high summer temperatures in SCAA and NCAA, up to 1.8 and 2.5°C warmer than the 1958–1995 mean (Figure 6c). Since 1996, significant warming trends are found\ref{} in SCAA (+0.06 ± 0.03°C/year) and NCAA (+0.10 ± 0.04°C/year). Sharp et al. (2011b) indicate that the recent increase in summer temperatures leads to early melting of the snow cover in CAA ablation zones, exposing bare ice for longer periods during the melt season and enhancing runoff.

Figure 6c reveals a significant anticorrelation between 2 m temperature in NCAA ($R^2 = 0.70$, p value = 4.4×10^{-6}) and SCAA ($R^2 = 0.63$, p value = 3.1×10^{-5}) and the North Atlantic Oscillation (NAO) index for the period 1996–2015 (http://www.cpc.ncep.noaa.gov). During 1996–2015, a negative NAO index prevailed in summer,

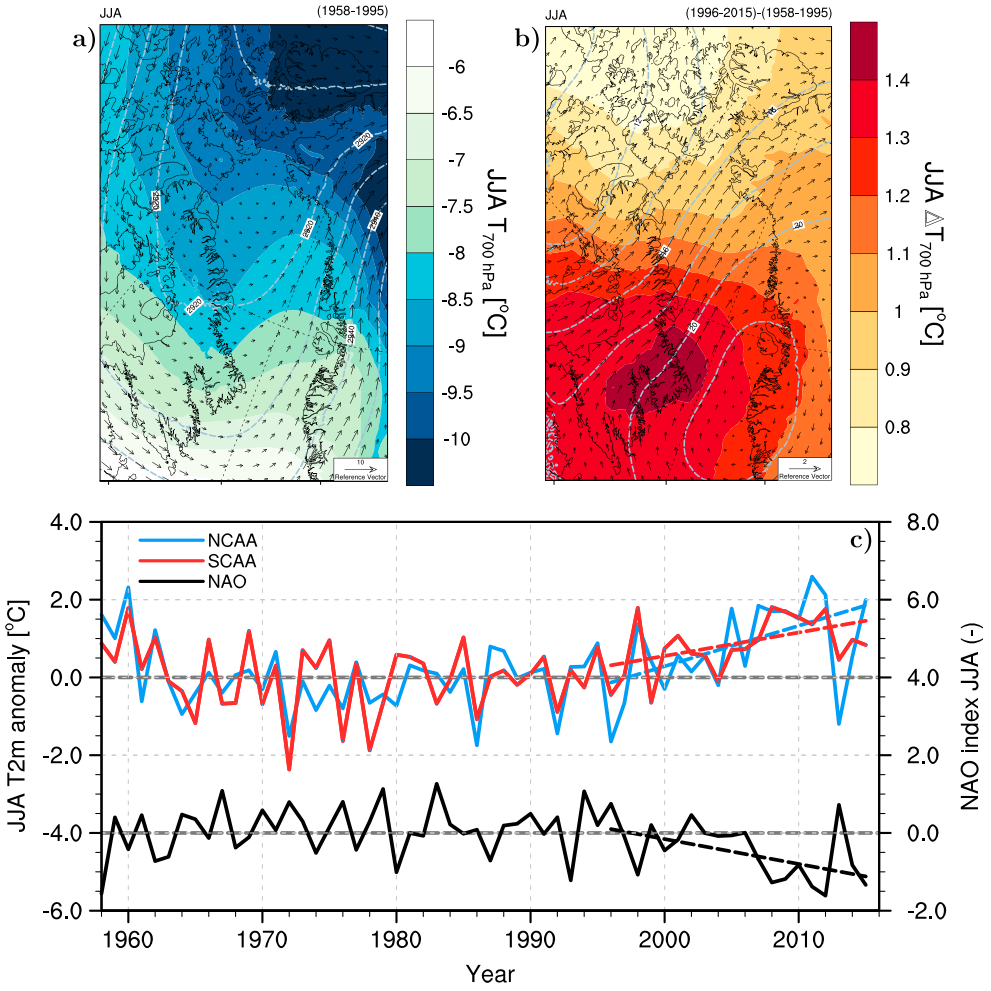

Figure 6. (a) Average June-July-August (JJA) temperature at 700 hPa for 1958–1995 from RACMO2.3. Mean wind direction is displayed as black arrows with superimposed 700 hPa geopotential heights (m; dashed grey). Wind speed (m/s) can be estimated using the reference vector shown at the bottom right corner of the map. (b) Changes in JJA mean temperature at 700 hPa (1996–2015 minus 1958–1995). Changes in mean wind speed and direction and 700 hPa geopotential heights are also shown. (c) Anomalies in JJA mean 2 m temperature for NCAA (blue) and SCAA (red), and JJA mean NAO index (black; http://www.cpc.ncep.noaa.gov). Anomalies are calculated with respect to the period 1958–1995. Dashed lines show trends for the period 1996–2015. RACMO2.3 = Regional Atmospheric Climate Model version 2.3; NCAA = Northern Canadian Arctic Archipelago; SCAA = Southern Canadian Arctic Archipelago; NAO = North Atlantic Oscillation.

that is, anomalously high pressure over the North Atlantic, which may be linked to the sea ice retreat and the associated increase in sea surface temperature in Davis Strait (Jaiser et al., 2012; Noël et al., 2014; Overland & Wang, 2010). Comparably negative summertime NAO values occurred in the period 1950–1960 (average NAO index −0.4), peaking in 1957 (−1.1), and in 1958 (−1.6, Figure 6c). These early episodes of negative NAO showed CAA summer 2 m temperature anomalies (Figure 6c) and mass loss (Figures 5a and 5b) similar to 1996–2015. Early mass loss was also reported by Zdanowicz et al. (2012) who found ice layers formed in the late 1950s in firn cores drilled in the summit region of Penny ice cap.

4.2. Before the Warming (1958–1995)

Prior to 1996, accumulation from precipitation accounts for 29 and 20 Gt/year in NCAA and SCAA (Tables 1 and 2 for numbers in mm w.e./year). Meltwater production, that is, 51 Gt/year in NCAA and 42 Gt/year in SCAA, exceeds precipitation by almost a factor of 2, highlighting the importance of refreezing to sustain CAA glaciers. For NCAA, high melt rates are restricted to the marginal regions, whereas melt propagates higher up on SCAA glaciers due to their lower elevation and higher near-surface temperature (Figure 7a). Unlike NCAA, runoff occurs over all but the very highest sectors of SCAA glaciers (Figure 7c), indicating a long-term dete-

Table 1
NCAA-Integrated MB, That Is, the Difference Between SMB and Solid Ice Discharge (3.5 ± 0.5 Gt/year)[a] and SMB Components (Top) and Trends (Bottom) for the Periods 1958–1995 and 1996–2015

Mean	Units	MB	SMB	RU	PR	ME	RF
1958–1995	Gt/year	−11.9 ± 11.5	−8.4 ± 11.0	36.7	28.7	50.5	20.8
1996–2015	Gt/year	−28.2 ± 11.5	−24.7 ± 11.0	53.5	29.0	68.3	23.0
1958–1995	mm w.e./year	−114 ± 110	−80 ± 105	352	275	484	199
1996–2015	mm w.e./year	−270 ± 110	−237 ± 105	513	278	654	220
Trend	Units	MB	SMB	RU	PR	ME	RF
1958–1995	Gt/year^2	—	0.44 ± 0.25	−0.36 ± 0.22	0.08 ± 0.06	−0.28 ± 0.24	0.02 ± 0.04
1996–2015	Gt/year^2	—	−2.06 ± 0.77	1.85 ± 0.64	−0.23 ± 0.21	2.03 ± 0.72	0.10 ± 0.11

Note. SMB components include runoff (RU), total precipitation (PR), total melt (ME) and refreezing (RF). NCAA = Northern Canadian Arctic Archipelago; MB = mass balance; SMB = surface mass balance.
[a]Millan et al., 2017.

rioration of the firn refreezing capacity (Figure 7b). In SCAA, the firn only retains 32% (13.4 Gt/year) of the melt while the healthier firn area of NCAA ice caps buffers 41% of melt through refreezing (20.8 Gt/year). As a result, prior to 1996 NCAA ice caps remained closer to balance (−114 ± 110 mm w.e./year) than SCAA glaciers, which had already suffered significant mass losses (275 ± 104 mm w.e./year) since the early 1980s. However, because NCAA glaciers cover a much larger area than SCAA ones, their integrated mass loss is similar with 11.9 ± 11.5 Gt/year and 11.9 ± 4.5 Gt/year respectively. Such long-term mass loss in SCAA has previously been reported by Gardner et al. (2012), who estimated the mass loss for 1963–2006 to be 11 ± 3 Gt/year, using altimetry measurements and stereographic images; the downscaled product provides similar results with an average mass loss of 10.9 ± 4.5 Gt/year for that period.

4.3. Mass Loss Acceleration (1996–2015)

During the last two decades, summer 2 m temperature increased by about 1.1°C (Figures 5c and 6c), more than doubling and doubling the pre-1996 mass loss of NCAA (28.2 ± 11.5 Gt/year) and SCAA (22.0 ± 4.5 Gt/year) respectively. In NCAA, a combination of increased runoff (+1.9 Gt/year^2) and reduced precipitation (−0.2 Gt/year^2) contributes to accelerated mass loss (2.1 Gt/year^2), whereas SCAA mass loss acceleration (1.0 Gt/year^2) is exclusively driven by enhanced runoff (+1.0 Gt/year^2; Tables 1 and 2). To investigate the spatial impact of the recent warming, Figures 7d–7f show the changes in melt, refreezing, and runoff after 1996 (1996–2015 minus 1958–1995). It also reveals a striking contrast: although SCAA experienced a smaller warming (Figures 5c and 6c), the increase in melt is larger than in NCAA (Figure 7d). In SCAA, decades of high melt rates have progressively depleted the firn pore space, reducing the ability to buffer the additional meltwater (+0.8 Gt/year^2) through refreezing (−0.1 Gt/year^2). As a result, all elevations experience enhanced runoff (Figure 7f). In contrast, the elevated firn layers of NCAA experience no additional runoff as enhanced

Table 2
SCAA-integrated MB, That is, the Difference Between SMB and Solid Ice Discharge (0.06 Gt/year)[a] and SMB Components (Top) and Trends (Bottom) for the Periods 1958–1995 and 1996–2015

Mean	Units	MB	SMB	RU	PR	ME	RF
1958–1995	Gt/year	−11.9 ± 4.5	−11.8 ± 4.5	32.0	20.4	41.9	13.4
1996–2015	Gt/year	−22.0 ± 4.5	−21.9 ± 4.5	43.9	21.9	52.3	13.3
1958–1995	mm w.e./year	−275 ± 104	−273 ± 104	740	472	969	310
1996–2015	mm w.e./year	−509 ± 104	−506 ± 104	1020	506	1210	308
Trend	Units	MB	SMB	RU	PR	ME	RF
1958–1995	Gt/year^2	—	0.23 ± 0.19	−0.16 ± 0.18	0.08 ± 0.04	−0.13 ± 0.17	0.04 ± 0.02
1996–2015	Gt/year^2	—	−1.00 ± 0.31	1.00 ± 0.33	−0.02 ± 0.09	0.82 ± 0.32	−0.10 ± 0.04

Note. SMB components include runoff (RU), total precipitation (PR), total melt (ME) and refreezing (RF). SCAA = Southern Canadian Arctic Archipelago; MB = mass balance; SMB = surface mass balance.
[a]Van Wychen et al. (2015).

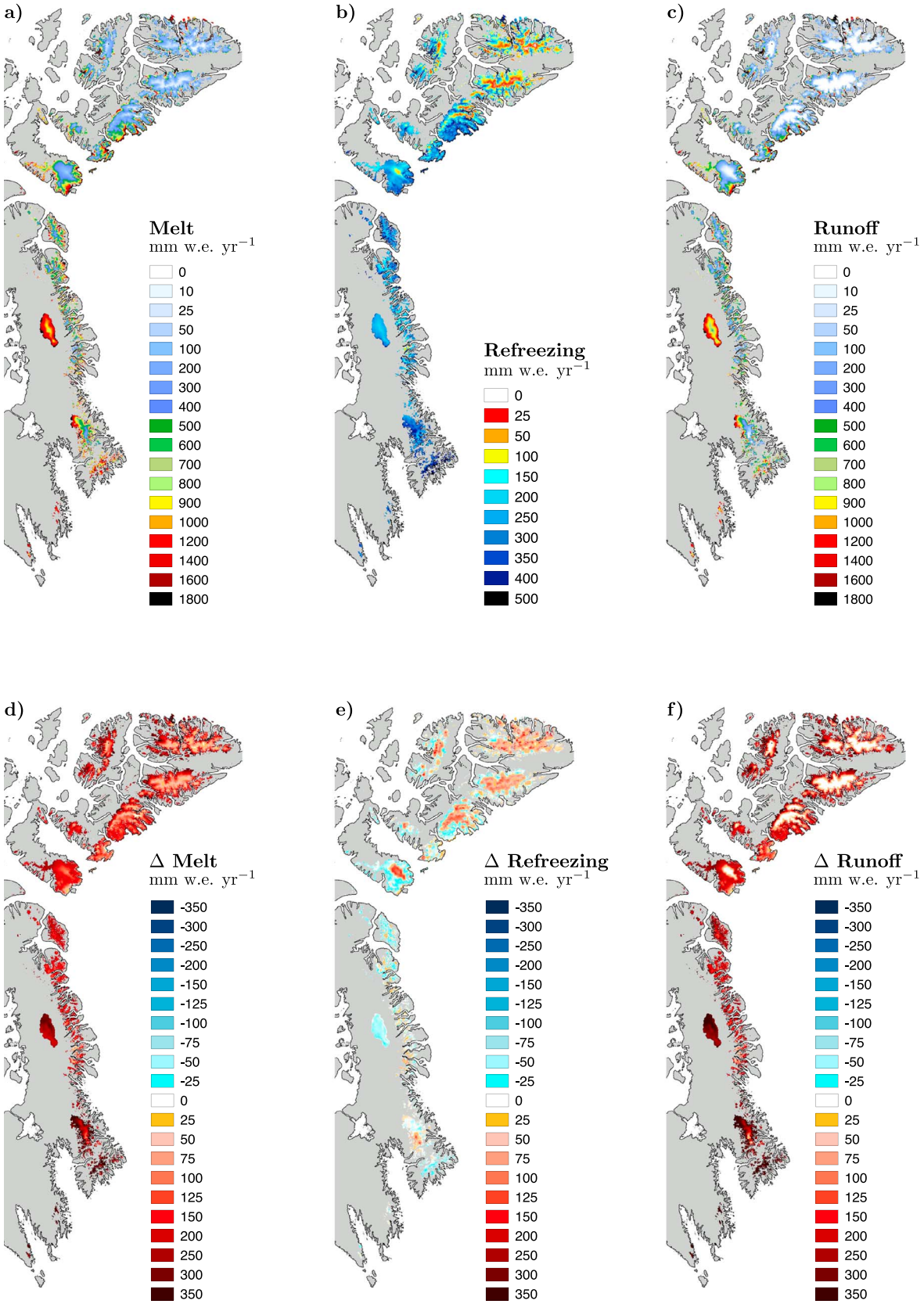

Figure 7. Mean (a) melt, (b) refreezing, and (c) runoff for the period 1958–1995. Changes in (d) melt, (e) refreezing, and (f) runoff after 1996 (1996–2015 minus 1958–1995). Tundra regions are displayed in light grey.

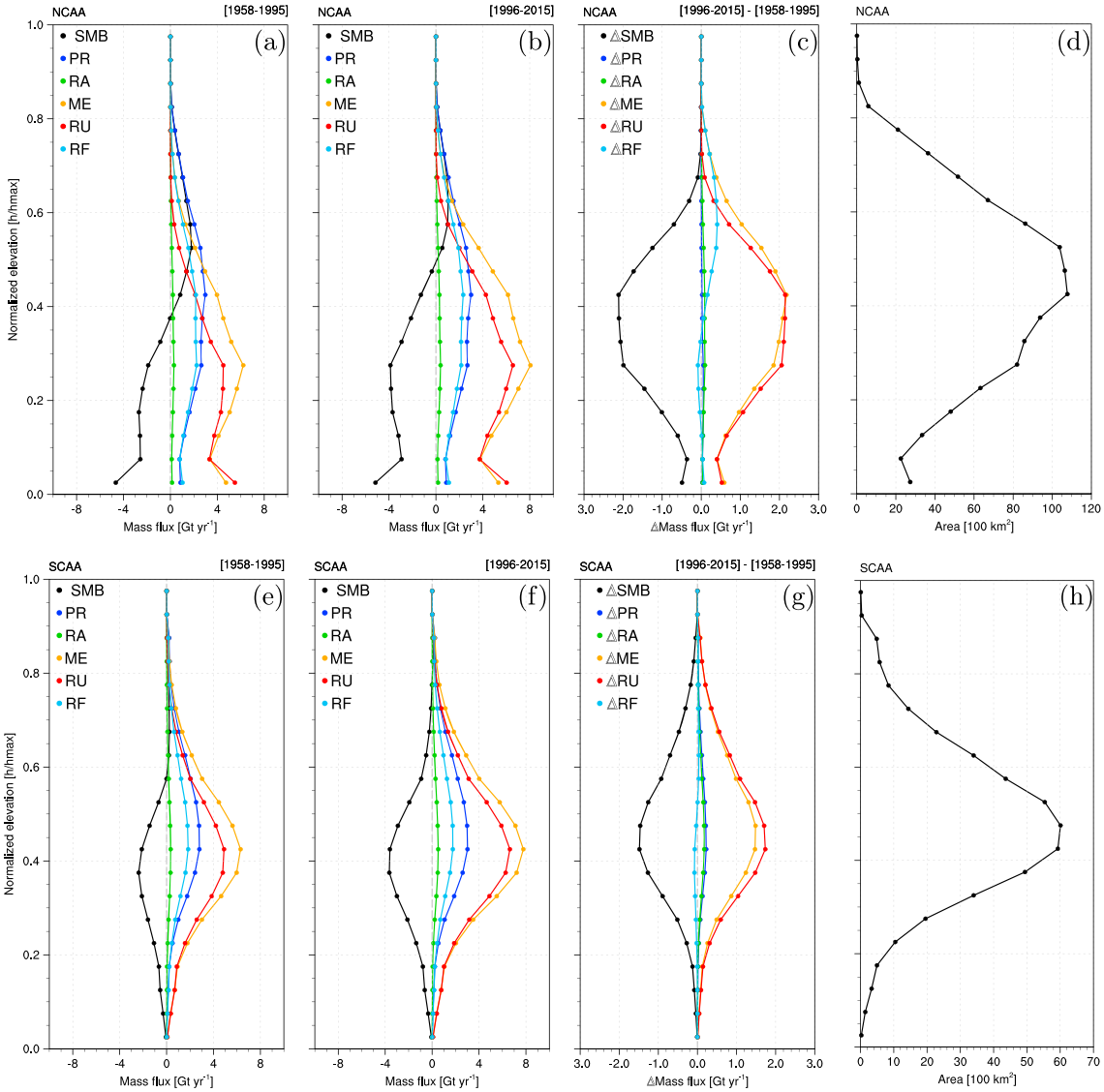

Figure 8. Vertical profiles of SMB components integrated over NCAA (top row) and SCAA (bottom row) elevation bins, scaled by the maximum height per region (h_{max}), for the period 1958–1995 (a and e), 1996–2015 (b and f), and the difference between the two periods (1996–2015 minus 1958–1995, c and g). SMB components are spatially integrated within normalized elevation bins (h/h_{max}) of magnitude 0.05. (d and h) The scaled hypsometries, that is, total area occupied by each elevation bin, for NCAA and SCAA, respectively. In NCAA and SCAA, h_{max} reaches 2,350 and 2,080 m, respectively. NCAA = Northern Canadian Arctic Archipelago; SCAA = Southern Canadian Arctic Archipelago; SMB = surface mass balance; PR = total precipitation; RA = rainfall; ME = total melt; RU = runoff, RF = refreezing.

melt (Figure 7d) is partly compensated by increased refreezing (Figure 7e). In SCAA, such mechanism is only found locally in the highest sectors of Bylot and Penny ice caps (Figure 7e).

5. Changes in the Firn Structure

To highlight the latitudinal contrast in meltwater retention regimes, Figure 8 shows scaled vertical profiles of SMB components integrated over elevation bins for individual NCAA and SCAA ice masses before (Figures 8a and 8e) and after (Figures 8b and 8f) 1996; the difference between the two periods (1996–2015 minus 1958–1995; Figures 8c and 8g) and the hypsometry of NCAA and SCAA (Figures 8d and 8h). Before 1996, NCAA ice caps are almost in balance with extensive accumulation zones above 0.5 of h_{max}, compensating for the mass lost in the ablation areas. In contrast, the ablation zone of SCAA glaciers already extended well above the peak in the hypsometry (0.5 of h_{max}), indicating continued mass loss at all elevations throughout the past six decades.

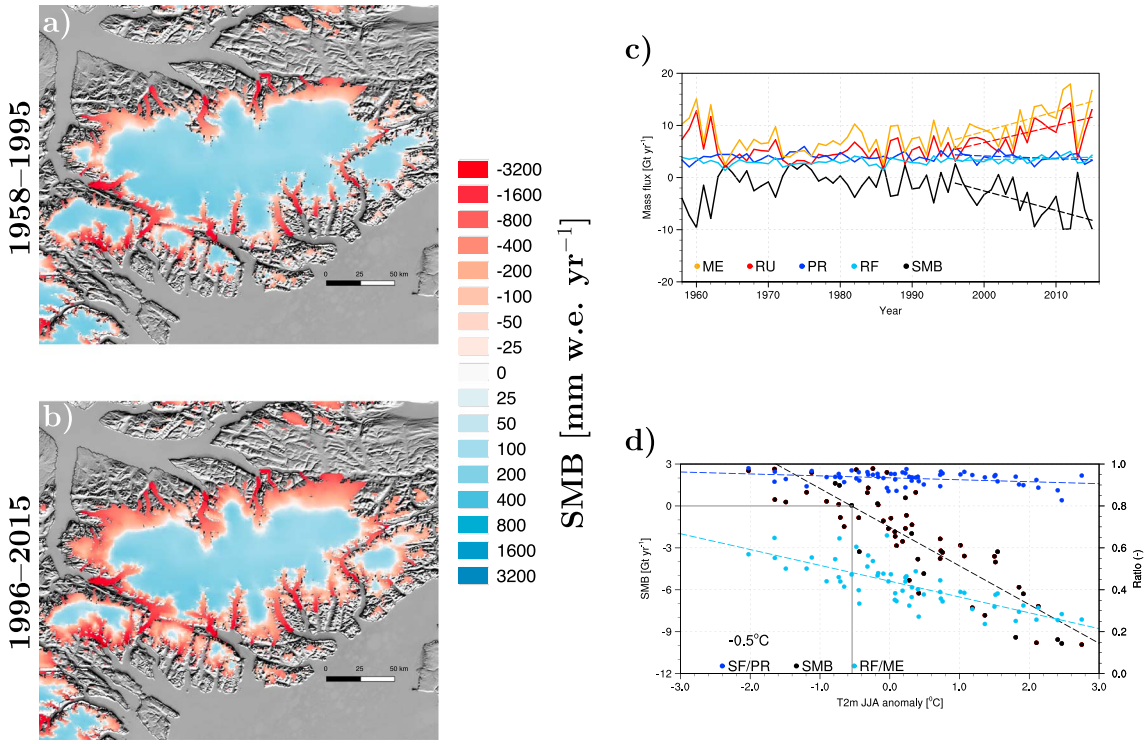

Figure 9. Maps of SMB at Agassiz ice cap averaged for periods (a) 1958–1995 and (b) 1996–2015. Time series of (c) SMB components, that is, melt (ME), runoff (RU), precipitation (PR), and refreezing (RF). (d) Annual SMB (black), snowfall-to-precipitation ratio (dark blue) and refreezing-to-melt ratio (light blue) as a function of the anomaly in mean JJA 2 m temperature, relative to the 1958–1995 mean. The vertical grey line estimates the JJA 2 m temperature anomaly relative to 1958–1995 needed to return Agassiz ice cap to mass balance (SMB = 0). SMB = surface mass balance; JJA = June-July-August.

From 1996 onward, the equilibrium line of NCAA moved upward, from ~0.35 to ~0.5 of h_{max}, beyond the peak in the hypsometry (Figure 8d). This means that only the most elevated firn zones of NCAA do not yet experience sustained mass loss, as increased meltwater is efficiently refrozen in available firn pore space, which mitigates the increase in runoff (Figure 8c). In SCAA, ablation now affects all sectors of the glaciers (Figure 8h). Decades of high meltwater production depleted pore space of the SCAA firn area, which is no longer able to buffer additional liquid water from enhanced melt and rain (Figure 8g). Therefore, runoff increases (+1.0 Gt/year^2, Table 2) at a greater rate than meltwater production (+0.8 Gt/year^2, Table 2). As a result, under continuous warming, SCAA glaciers are expected to undergo sustained and irreversible mass loss in the next decades. This mechanism has already been observed on Devon ice cap (Bezeau et al., 2013; Gascon et al., 2013), the southernmost ice body of NCAA, and upon further warming will propagate to higher latitudes.

6. Six Decades of Mass Loss in the Canadian Arctic Archipelago

Sections 6.1 to 6.4 focus on Agassiz ice cap (80°N, 75°W) located in the NCAA and the three major SCAA ice caps, Bylot Island ice cap (73°N, 78.5°W), Penny ice cap (67°N, 66°W), and Barnes ice cap (70°N, 73.5°W), respectively. Figures 9 to 12 show annual mean SMB for (a) 1958–1995, (b) 1996–2015, (c) time series of annual cumulative SMB components (1958–2015), and (d) integrated SMB, snowfall-to-precipitation and refreezing-to-melt fractions as a function of JJA 2 m temperature anomaly relative to the 1958–1995 mean. In the following sections, we assume mass loss to equal SMB as solid ice discharge remains small for these ice caps (Van Wychen et al., 2015, 2016).

6.1. Agassiz Ice Cap

Agassiz ice cap measures ~21,000 km^2 and is located to the north east of Ellesmere Island in the NCAA. The ice cap shows a long-term ELA at ~1,100 m a.s.l. (above sea level), and its summit reaches ~1,980 m a.s.l. (Gray et al., 2015). Agassiz is drained by several marine-terminating glaciers covering roughly 40% of the ice cap area (Millan et al., 2017). Williamson et al. (2008) and Van Wychen et al. (2016) estimated the mean solid ice

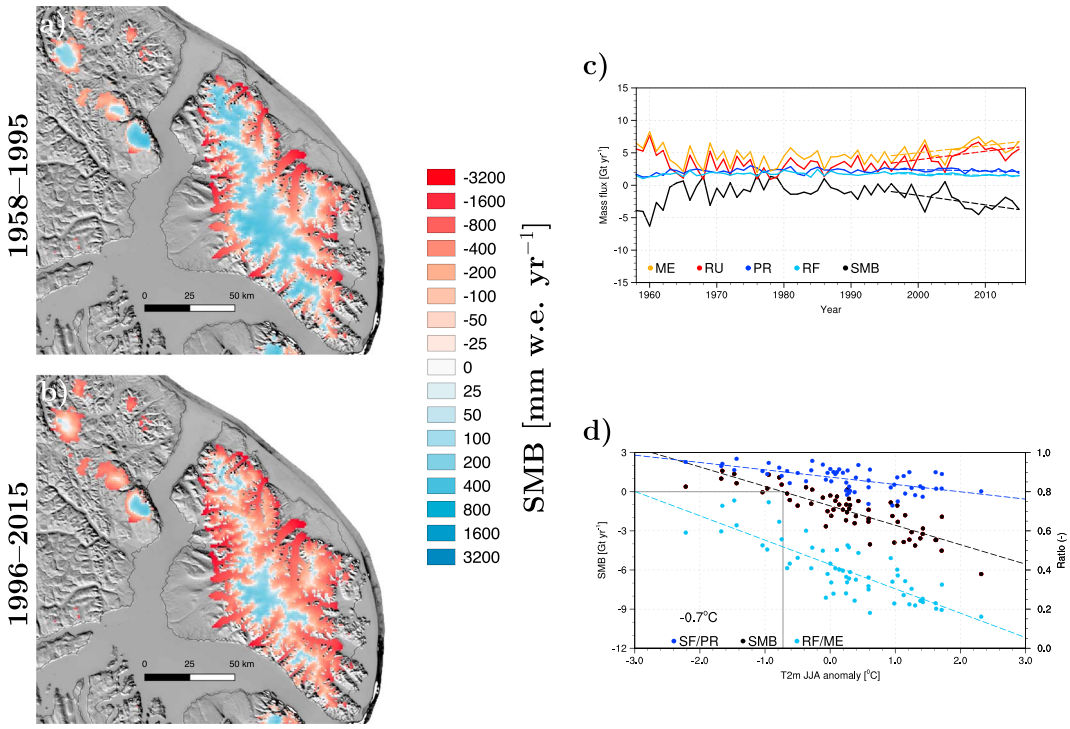

Figure 10. As in Figure 9 but for Bylot island. SMB = surface mass balance; JJA = June-July-August.

discharge at 0.41 ± 0.08 Gt/year for 1999–2002 and 0.12 ± 0.07 for 2000–2015, respectively. This is in line with Millan et al. (2017) who estimated a slowdown of ice discharge by 60% between the periods 1990–2010 (0.28 ± 0.05 Gt/year) and 2010–2015 (0.11 ± 0.05 Gt/year), with no significant change after 2000 at four major marine-terminating glaciers.

Owing to an extensive accumulation zone (Figure 9a), Agassiz ice cap remained almost in balance before the recent warming in 1996 with an average mass loss of ~1.3 Gt/year (Figure 9c). Mass loss is restricted to narrow ablation zones and marine outlet glaciers and is primarily driven by meltwater runoff (5.2 Gt/year) that exceeds precipitation (4.0 Gt/year). In this early period, 41% of surface melt (7.2 Gt/year) is retained in the inland firn zone. After 1996, surface melt increased by 46% (10.6 Gt/year) affecting not only the marginal ablation zones but also the highest sectors of the ice cap (Figure 7d). In the elevated firn zone, this additional meltwater is efficiently buffered through enhanced refreezing (+18% after 1996 and contributing 3.5 Gt/year on average). As a result, increased runoff (+57%; 8.2 Gt/year) is restricted to marginal ablation zones which slightly propagated inland, more than tripling the pre-1996 mass loss (4.2 Gt/year). Using repeat airborne laser altimetry records from 1995 and 2000, Abdalati et al. (2004) show an ice cap wide thinning of 0.07 m/year, dominated by ice loss in marginal ablation zones with little changes in the ice cap interior. As a result, Agassiz ice cap has lost 2.0 Gt/year of ice during the 1995–2000 period, similar to the downscaling method suggesting 2.1 Gt/year.

Figure 9d shows that Agassiz ice cap has lost mass at an average rate of 2.8 Gt/°C for 1958–2015 (black dashed line). To return to balance (SMB = 0), Agassiz would require a summer (JJA) cooling of ~0.5°C compared to pre-1996 mean 2 m temperature (−1.0°C). Following a ~3°C summer warming relative to the 1958–1995 mean, a simultaneous snowfall decrease (10%) and higher melt production could reduce the firn refreezing capacity by a factor of 2, that is, from 40% down to 20%, further decreasing SMB by 9 Gt/year.

6.2. Bylot Island

Bylot Island is the northernmost ice cap of SCAA, comprising a network of marginal surge-type glaciers (Van Wychen et al., 2015), with an ice thickness of up to 400 m (Van Wychen et al., 2016). The ice cap covers ~4,900 km^2, and its summit elevation is ~1,680 m. Despite an extensive inland accumulation zone, Figures 10a and 10c show that Bylot Island ice cap was already losing mass (1.0 Gt/year) before the recent warming. Significant runoff from marginal glaciers (3.2 Gt/year) exceeds the relatively low precipitation (2.2 Gt/year). In the early period, Bylot Island showed a similar regime as NCAA ice caps have today, with ~40% of total melt (4.4

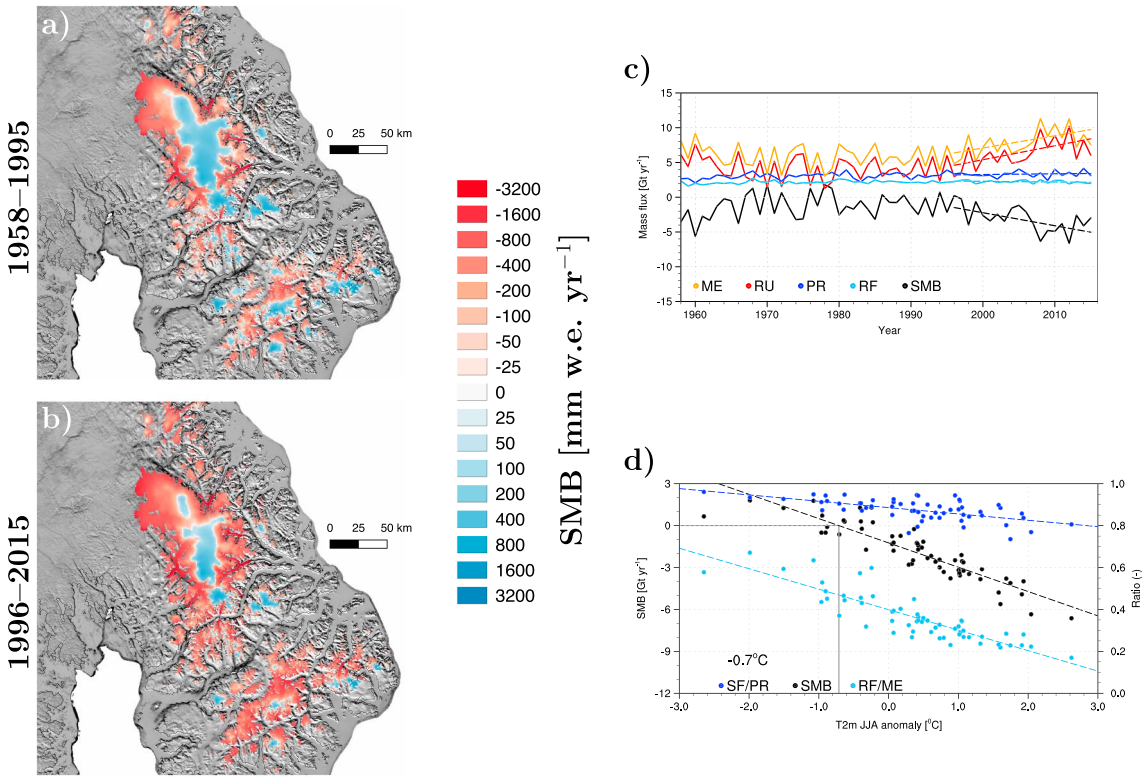

Figure 11. As in Figure 9 but for Penny ice cap. SMB = surface mass balance; JJA = June-July-August.

Gt/year) refrozen in the inland firn. In the last two decades, enhanced melt depleted the available pore space, reducing the refreezing capacity of the firn from 40% to 30%, significantly increasing runoff (+41% after 1996 and contributing 4.5 Gt/year on average). As a result, the accumulation zone withdrew to higher elevations (Figure 10b) and the mass loss doubled (2.2 Gt/year), indicating a recent acceleration. Mass loss measurements from combined stereographic images and satellite altimetry confirm that the average mass loss increased from 1.4 Gt/year in 1979–2008 (SPOT) and 1980–2006 (ICESat) to 2.7 Gt/year in 2003–2009 (ICESat, Gardner et al., 2012), in line with 1.1 and 2.3 Gt/year derived from the downscaled SMB product.

Over 1958–2015, Bylot ice cap lost 1.5 Gt of ice per °C warming on average (Figure 10d) and a summer cooling of ~0.7°C relative to the average 2 m temperature of the pre-1996 period (−1.2°C) would be required to bring the ice cap back in balance. Figure 10d also highlights an increase in liquid at the expense of solid precipitation, further deteriorating the buffer capacity of the firn layer. Extrapolating the regression in Figure 10d suggests that Bylot Island's refreezing capacity is fully lost for summer temperatures ~3°C higher than the 1958–1995 average.

6.3. Penny Ice Cap

Penny ice cap is a remnant of the Laurentide ice sheet, located on southern Baffin Island (Zdanowicz et al., 2002). It is composed of a large central ice mass (~6,500 km^2) feeding several valley glaciers of which two are marine terminating, that is, Coronation Glacier in the east and an unnamed glacier in the north. Penny ice cap is the only southern ice body that has a sufficiently elevated interior (up to 1,930 m) to enable the formation of a perennial firn zone (Figure 11a; Zdanowicz et al., 2012). Satellite observations indicate that Penny ice cap has already been losing mass for several decades (Gardner et al., 2012), that is, 1.5 Gt/year for 1958–2006 (ICESat) and 1.1 Gt/year for 1958–2009 (SPOT). This is in line with our results: 1.4 and 1.6 Gt/year, respectively. Prior to the recent warming in 1996, mass loss was mostly concentrated on marginal outlet glaciers and in the wide, gently sloping northwestern ablation zone (Figure 11a). Mass loss (1.3 Gt/year) resulted from runoff (4.2 Gt/year) exceeding precipitation (3.0 Gt/year), although 37% of total melt (5.2 Gt/year) was refrozen in the snowpack (Figure 11c). After 1996, ablation propagates further inland, restricting the accumulation zone to the highest sectors (Figure 11b). Intensified melt (+33% after 1996 and contributing 7.8 Gt/year on average) and reduced refreezing

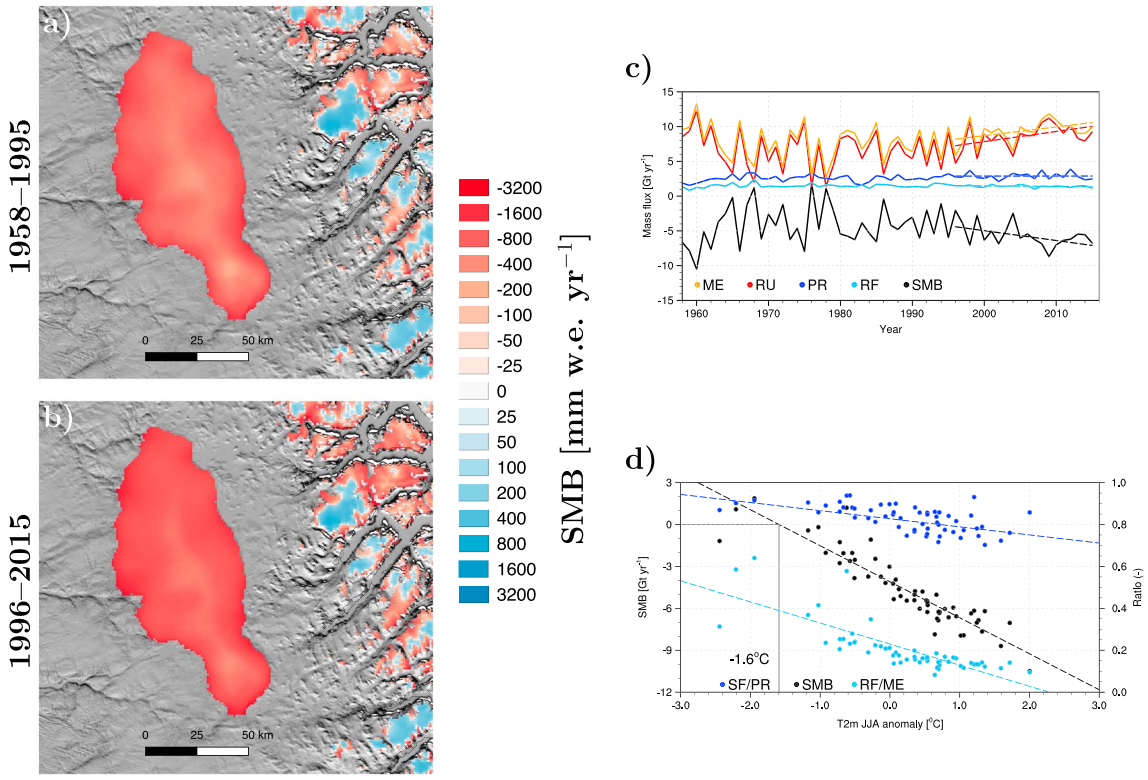

Figure 12. As in Figure 9 but for Barnes ice cap. SMB = surface mass balance; JJA = June-July-August.

capacity (−8%; 28%) enhanced runoff by 50% (6.3 Gt/year). As a result, the pre-1996 mass loss increased 2.5 fold (3.1 Gt/year), signifying mass loss acceleration. Satellite measurements showing accelerated mass loss from 1.3 and 2.9 Gt/year for 1995–2000 and 2000–2005 (ATM) and 3.3 Gt/year in 2003–2009 (ICESat, Gardner et al., 2012) are in line with our results: 1.6, 2.4, and 3.3 Gt/year for the three periods.

Similar to Bylot Island, Penny ice cap lost 1.7 Gt of ice per °C warming (Figure 11d). Here a summer cooling of ∼0.7°C with respect to the average 1958–1995 near-surface temperature (−2.0°C) is needed to sustain the ice cap. In addition, Figure 11d highlights the sensitivity of Penny ice cap to increased summer temperature; a summer warming of ∼3°C leads to ∼20% more liquid precipitation at the expense of snowfall, reducing the refreezing capacity of Penny's firn zone to about 10% and hence decreasing SMB by ∼6 Gt/year. Similar to Bylot Island, Penny ice cap's refreezing capacity will inevitably collapse in a warming climate (+4°C relative to 1958–1995; Figure 11d).

6.4. Barnes Ice Cap

Covering an area of ∼5,900 km^2, Barnes ice cap is another remnant of the Laurentide ice sheet (Gilbert et al., 2017) that is located ∼400 km to the northwest of Penny ice cap. It comprises three main domes, with a maximum ice thickness of 550 m (Clough & Løken, 1968) and is surrounded by outlet glaciers terminating in proglacial lakes. These glaciers contribute to Barnes ice cap mass loss through active calving (Andrews et al., 2002). Unlike Penny ice cap, Barnes ice cap is too low (summit at 1,120 m) to preserve a perennial firn zone. As a result, Barnes only sporadically accumulates mass from superimposed ice (Baird, 1952; Hooke et al., 1987). At lower elevations, a combination of white, blue, intermediate, or debris-covered ice can be found; these regions also show meltwater lakes in depressions, reminiscent of previous surging glacier activity (Holdsworth, 1977).

Figures 12a and 12b show that Barnes ice cap has been undergoing uninterrupted mass loss in the last 58 years (Figure 12c). During the period 1958–1995, precipitation (2.5 Gt/year) only forms a shallow snow cover, in which little refreezing (1.5 Gt/year) takes place. Therefore, 86% of surface melt (7.7 Gt/year) runs off (6.7 Gt/year) toward marginal proglacial lakes. This early mass loss is confirmed by Gardner et al. (2012), who estimated the 1960–1995 (ATM) mass loss at 1.9 Gt/year. As the downscaling method uses a contemporary (2000–2015), darker MODIS ice albedo product to correct melt, mass loss is generally overestimated prior to the 2000s (4.0 Gt/year for 1960–1995). As argued in Noël et al. (2016), too low ice albedo values in MODIS

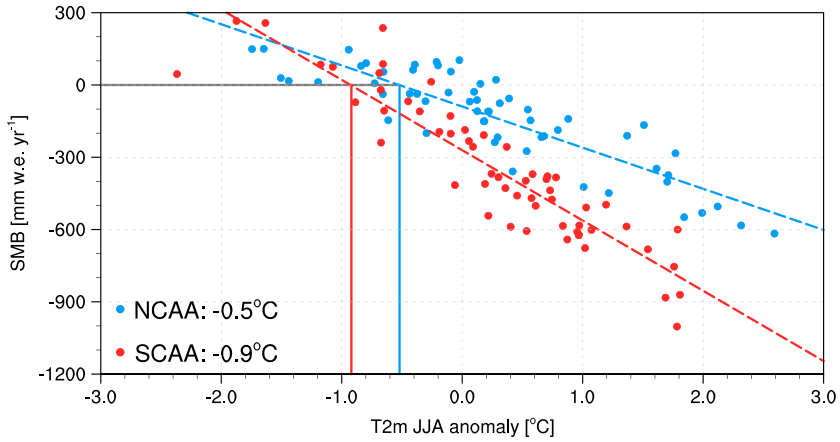

Figure 13. SMB as a function of anomaly in JJA 2 m temperature, relative to the 1958–1995 mean, for integrated NCAA (blue) and SCAA (red) ice caps. Dashed lines represent linear SMB-to-temperature regressions; the vertical lines estimate the JJA 2 m temperature anomaly relative to 1958–1995 needed to return NCAA (blue) and SCAA (red) ice caps to mass balance (SMB = 0). SMB = surface mass balance; JJA = June-July-August; NCAA = Northern Canadian Arctic Archipelago; SCAA = Southern Canadian Arctic Archipelago.

images could result from bright ice pixels being mixed with neighboring darker wet ice or meltwater lakes. This discrepancy tends to disappear in the more recent period.

After 1996, mass loss from Barnes ice cap started to accelerate as reported by three successive satellite records (ATM, Gardner et al., 2012): 3.4 Gt/year (1995–2000), 4.2 Gt/year (2000–2005), and 6.3 Gt/year (2005–2011). The downscaled product shows similar results with 4.7, 5.3, and 6.7 Gt/year for the three periods. Following the recent warming, runoff increased by 27% (8.5 Gt/year) as a consequence of combined melt increase (+20% after 1996 and contributing 9.3 Gt/year on average) and reduced refreezing capacity (−4%; 15%). In contrast to Bylot and Penny ice caps, refreezing is almost exclusively driven by winter snowfall accumulation, which decreased by ~5%.

Barnes is also ~40% more sensitive to summer warming than Bylot and Penny ice caps and loses −2.6 Gt of ice per °C (Figure 12d). Relative to the 1958–1995 average (−0.3°C), Barnes ice cap would require a JJA cooling of 1.6°C to return to balance. Figure 12d also suggests that a 2°C summer warming will lead to an ~30% decrease in solid precipitation and would terminate all liquid water retention at Barnes ice cap. In a recent study, Gilbert et al. (2017) predicted the total disappearance of Barnes ice cap in the next 300 years.

6.5. CAA Climate Sensitivity

Figure 13 shows the sensitivity of NCAA (blue) and SCAA (red) SMB to summer warming with respect to the 1958–1995 period. Owing to increased refreezing of meltwater in firn, the healthier NCAA ice caps would only need half the required SCAA summer cooling to return back to balance, with 0.5 and 0.9°C, respectively. As a result, SCAA ice caps show a mass loss response to summer warming (292 mm w.e./°C) larger than that of the NCAA (171 mm w.e./°C). This difference reveals a pronounced latitudinal contrast: while SCAA ice caps rapidly lose mass from superimposed ice, NCAA ice bodies still mitigate mass loss through active refreezing in firn but will likely undergo significant acceleration in the near future as enhanced melt progressively depletes the remaining pore space, drastically increasing meltwater runoff.

Although overly simplistic, that is, no elevation or glacier retreat feedback is considered, we use a linear regression between SMB and summer 2 m temperature anomaly (black dashed line in Figures 9–12e) to study the scales of enhanced mass loss for the four ice caps in a future warming climate. By the end of the 21st century (2011–2100), for a moderate warming scenario (RCP 4.5), Lenaerts et al. (2013) predict an increase in CAA near-surface temperature of about 6.5°C. As a result, mass loss would increase by 18.2 Gt/year (14×), 9.8 Gt/year (10×), 11.1 Gt/year (9×) and 16.9 Gt/year (4×) relative to the 1958–1995 average for Agassiz, Bylot, Penny, and Barnes ice caps, respectively.

At the current rate of mass loss (MB in Tables 1 and 2), that is, the difference between SMB and solid ice discharge, NCAA ice caps ($22.4 - 37.6 \times 10^3$ Gt of ice; Vaughan et al., 2013) contribute 0.08 ± 0.03 mm/year to ongoing sea level rise and could survive for another 800 to 1,400 years, whereas the highly sensitive SCAA

glaciers (5.5–8.8 $\times 10^3$ Gt of ice; Vaughan et al., 2013) are currently responsible for 0.06 ± 0.01 mm/year and would totally disappear within 250 to 400 years.

7. Limitations

Statistical downscaling is an invaluable tool to resolve local SMB patterns over the small CAA ice bodies. However, this technique suffers from several limitations:

1. The performance of the downscaled product strongly depends on the quality of the input data. Here we use modeled SMB components from RACMO2.3, known to underestimate meltwater runoff in low-lying regions resulting from, for example, too low marginal turbulent heat fluxes (Noël et al., 2015). In addition, the model uses a relatively coarse topography (GTOPO30) and glacier outlines (Global Land Cover Characteristics) to estimate the SMB elevation gradients. Inaccuracies in modeled gradients inherently lead to biases in the downscaled product. To address this issue, an updated DEM will be used in forthcoming CAA climate simulations. Nevertheless, Lenaerts et al. (2013) showed that this DEM could be used to model realistic SMB over the CAA ice caps, with generally good agreement when compared to in situ measurements and GRACE mass change.
2. Precipitation does depend not only on surface elevation, that is, near-surface temperature, but also on wind speed and direction affecting precipitation distribution and air moisture content determining the accumulation total. Statistical downscaling cannot account for these additional physical processes, and precipitation is therefore bilinearly interpolated to the 1 km glacier outline without altering the modeled precipitation field. Further improvements could be obtained by dynamically downscaling precipitation, that is, using a simulation at higher spatial resolution, for example, 5.5 km, explicitly solving the physics and dynamics of the atmosphere and interactions with the ice surface topography.
3. The underestimation of cloud optical thickness in RACMO2.3 leads to SW_d being overestimated, potentially overestimating melt through the ice albedo correction.
4. The downscaled melt and runoff estimates rely on the quality of the MODIS product used for the ice albedo correction. The average 1 km MODIS ice albedo product remains constant in time and is representative for the period 2000–2015. Therefore, bare ice albedo might be underestimated prior to 2000 as the period 2000–2015 includes record high melt years. As discussed in section 3.2.1, marginal floating glacier tongues generally show underestimated albedo values in MODIS, resulting from a mixed signal from dark meltwater ponds and crevasses and the surrounding brighter ice captured in a same MODIS cell. In addition, Polashenski et al. (2015) and Casey et al. (2017) showed that the deterioration of MODIS sensor tends to underestimate surface albedo records, hence overestimating melt in the downscaled product.
5. The inability to discriminate between snow-covered and bare ice surfaces at 1 km resolution on a daily basis. Therefore, the downscaling procedure applies the ice albedo correction irrespective of the surface conditions, that is, even when a shallow snow cover persists few days in the ablation zone in summer.

As a result, additional ice melt (ME_{add}) is overestimated, leading to a relatively low f_{scale} value (0.2). This indicates that only 20% of the additional melt must run off to optimize the agreement of the downscaled product with in situ SMB measurements, while the remainder must be retained through refreezing. This low f_{scale} value stresses the need for further development of the downscaling method and for improved quality of the different forcing data. Solving these limitations, statistical downscaling could be applied to glaciers and ice caps with sparse in situ measurements, for example, Patagonia, assuming $f_{scale} \approx 1$.

8. Conclusions

We use a new, 1 km daily SMB product to show that glaciers and ice caps in the CAA have been losing mass for decades. The downscaled product realistically resolves local SMB patterns of small glacierized features, such as narrow outlet glaciers and small ice fields, and has been successfully evaluated using in situ and remote sensing observations.

The SMB of CAA ice masses is primarily controlled by runoff, mitigated by the ability of elevated firn layers to only modestly buffer meltwater through refreezing. While refreezing kept NCAA ice caps near balance until the mid-1990s (−11.9 ± 11.5 Gt/year), SCAA glaciers already suffered sustained mass loss since the early 1980s (11.9 ± 4.5 Gt/year). During the last two decades, a shift in the regional circulation toward more frequent occurrence of persistent anticyclonic conditions favored warm southwesterly air advection toward

CAA glaciers. As a result, successive record warm summers raised the mean near-surface temperature of CAA by 1.1°C, more than doubling (28.2 ± 11.5 Gt/year) and doubling (22.0 ± 4.5 Gt/year) the pre-1996 glacial mass loss in NCAA and SCAA, respectively. This recent mass loss acceleration is independently confirmed by satellite altimetry and gravimetry measurements.

For NCAA ice caps, enhanced melt starts to deplete the available pore space of the extensive inland firn, progressively moving the accumulation zones to higher elevations. In SCAA, decades of sustained high melt rates have already deteriorated the firn refreezing capacity to such an extent that runoff accelerates at a faster pace than meltwater production. In a future warming climate, the healthier NCAA ice caps will continue to mitigate mass loss acceleration through increased refreezing until the buffering mechanism collapses. In contrast, the lower-lying SCAA glaciers are expected to undergo irreversible mass loss in the next decades and might totally disappear within 400 years.

Acknowledgments

B. Noël, W. J. van de Berg, B. Wouters, and M. R. van den Broeke acknowledge support from the Polar Programme of the Netherlands Organization for Scientific Research (NWO/ALW) and the Netherlands Earth System Science Centre (NESSC). All data are available from authors without conditions. Mass balance measurements from the Meighen, Agassiz, Penny, and Devon ice caps were conducted under the Climate Change Geoscience Program (Geological Survey of Canada, Natural Resources Canada) and under McGill University for White Glacier. Logistical support for all fieldwork was provided by the Polar Continental Shelf Project (Natural Resources Canada). We thank the Nunavut Research Institute, Aurora Research Institute, and northern communities for granting permission to conduct research on ice caps and glaciers in the CAA. This compilation of SMB measurements was first published in Gardner et al. (2011). Mass change estimates derived from ICESat and CryoSat-2 are freely available from the authors upon request. Annual mean SMB, total precipitation (from rain and snowfall), total melt (from snow and ice), and runoff (mm w.e./year) covering the NCAA and SCAA at 1 km resolution and averaged for the two periods 1958–1995 and 1996–2015, respectively, can be freely downloaded from PANGAEA at https://doi.org/10.1594/PANGAEA.881315. The daily, 1 km SMB data set and associated components for both NCAA and SCAA (1958–2015) are available from the authors without conditions upon request. B. N. prepared the manuscript, carried out the RACMO2.3 simulation, and produced the downscaled data sets at 1 km for NCAA and SCAA, respectively. B. N., W. J. B., and M. R. B. conceived the downscaling procedure and analyzed the data. W. J. B. carried out the hypsometry change sensitivity experiments. N. S. kindly provided unpublished SMB measurements over Penny ice cap in the SCAA. S. L. processed the 1 km MODIS albedo product. B. W. produced and analyzed the ICESat/CryoSat-2 data sets. All authors commented on the manuscript.

References

Abdalati, W., Krabill, W., Frederick, E., Manizade, S., Martin, C., Sonntag, J., et al. (2004). Elevation changes of ice caps in the Canadian Arctic Archipelago. *Journal of Geophysical Research*, *109*, F04007. https://doi.org/10.1029/2003JF000045

Andrews, J. T., Holdsworth, G., & Jacobs, J. D. (2002). Glaciers of the Arctic Islands. Glaciers of Baffin Island. *USGS Professional Paper*, *1386-J-1*, J162–J198.

Baird, P. D. (1952). Method of nourishment of the Barnes ice cap. *Journal of Glaciology*, *2*, 2–9.

Bezeau, P., Sharp, M., Burgess, D., & Gascon, G. (2013). Firn profile changes in response to extreme 21st-century melting at Devon Ice Cap, Nunavut, Canada. *Journal of Glaciology*, *59*, 981–991. https://doi.org/10.3189/2013JoG12J208

Budd, W. F., Keage, P. L., & Blundy, N. A. (1979). Empirical studies of ice sliding. *Journal of Glaciology*, *23*(89), 157–170. https://doi.org/10.1017/S0022143000029804

Casey, K. A., Polashenski, C. M., Chen, J., & Tedesco, M. (2017). Impact of MODIS sensor calibration updates on Greenland ice sheet surface reflectance and albedo trends. *The Cryosphere*, *11*, 1781–1795. https://doi.org/10.5194/tc-11-1781-2017

Clough, J. W., & Løken, O. H. (1968). Radio-echo sounding on the Barnes ice cap, *North-central Baffin Island field report 1967*, *Report Series 2* (pp. 87–102). Canada Department of Energy, Mines and Resources, Inland Waters Branch.

Cogley, J. G., Hock, R., Rasmussen, L. A., Arendt, A. A., Bauder, A., Braithwaite, R. J., et al. (2011). Glossary of glacier mass balance and related terms, technical documents in hydrology, IHP-VII technical documents in hydrology no. 86, IACS contribution no. 2, UNESCO-IHP, Paris.

Dee, D. P., Uppala, S. M., Simmons, A. J., Berrisford, P., Poli, P., Kobayashi, S., et al. (2011). The ERA-Interim reanalysis: Configuration and performance of the data assimilation system. *Quarterly Journal of the Royal Meteorological Society*, *137*, 553–597. https://doi.org/10.1002/qj.828

European Center for Medium-Range Weather Forecasts-Integrated Forecast System (2008). Part IV: Physical processes (CY33R1) (Tech. Rep.). ECMWF.

Ettema, J., van den Broeke, M. R., van Meijgaard, E., & van de Berg, W. J. (2010). Climate of the Greenland ice sheet using a high-resolution climate model - Part2: Near-surface climate and energy balance. *The Cryosphere*, *4*, 529–544. https://doi.org/10.5194/tc-4-529-2010

Gardner, A., Moholdt, G., Arendt, A., & Wouters, B. (2012). Accelerated contributions of Canada's Baffin and Bylot Island glaciers to sea level rise over the past half century. *The Cryosphere*, *6*(5), 1103–1125. https://doi.org/10.5194/tc-6-1103-2012

Gardner, A. S., Moholdt, G., Cogley, J. G., Wouters, B., Arendt, A. A., Wahr, J., et al. (2013). A reconciled estimate of glacier contributions to sea level rise: 2003 to 2009. *Science*, *340*(6134), 852–857. https://doi.org/10.1126/science.1234532

Gardner, A. S., Moholdt, G., Wouters, B., Wolken, G. J., Burgess, D. O., Sharp, M. J., et al. (2011). Sharply increased mass loss from glaciers and ice caps in the Canadian Arctic Archipelago. *Nature*, *473*, 357–360. https://doi.org/10.1038/nature10089

Gardner, A., & Sharp, M. (2009). Sensitivity of net mass-balance estimates to near-surface temperature lapse rates when employing the degree-day method to estimate glacier melt. *Annals of Glaciology*, *50*(50), 80–86. https://doi.org/10.3189/172756409787769663

Gascon, G., Sharp, M. J., Burgess, D. O., Bezeau, P., & Bush, A. (2013). Changes in accumulation area firn stratigraphy and meltwater flow during a period of climate warming, Devon Ice Cap, Nunavut, Canada. *Journal of Geophysical Research: Earth Surface*, *118*, 2380–2391. https://doi.org/10.1002/2013JF002838

Gesch, D. B., & Larson, K. S. (1998). Techniques for development of global 1-kilometer digital elevation models. In *Proc. Pecora Thirteenth Symposium*, CD-ROM, American Society for Photogrammetry and Remote Sensing, Bethesda, MD.

Gilbert, A., Flowers, G. E., Miller, G. H., Refsnider, K., Young, N. E., & Radić, V. (2017). The projected demise of Barnes Ice Cap: evidence of an unusually warm 21st century Arctic. *Geophysical Research Letters*, *44*, 2810–2816. https://doi.org/10.1002/2016GL072394

Government of Canada Natural Resources Canada Map Information Branch (2016). *Canadian digital elevation model product specifications edition 1.1*. Quebec, Canada: GeoGratis Client Services.

Gray, L., Burgess, D., Copland, L., Demuth, M. N., Dunse, T., Langley, K., & Schuler, T. V. (2015). CryoSat-2 delivers monthly and inter-annual surface elevation change for Arctic ice caps. *The Cryosphere*, *9*, 1895–1913. https://doi.org/10.5194/tc-9-1895-2015

Holdsworth, G. (1977). Surge activity on the Barnes Ice Cap. *Nature*, *269*(5629), 588–590.

Hooke, R. L., Johnson, G. W., Brugger, K. A., Hanson, B., & Holdsworth, G. (1987). Changes in mass balance, velocity, and surface profile along a flow line on Barnes Ice Cap, 1970-1984. *Canadian Journal of Earth Sciences*, *24*, 1550–1561.

Jaiser, R., Dethloff, K., Handorf, D., Rinke, A., & Cohen, J. (2012). Impact of sea ice cover changes on the Northern Hemisphere atmospheric winter circulation. *Tellus*, *64*, 11. https://doi.org/10.3402/tellusa.v64i0.11595

Lenaerts, J. T. M., van Angelen, J. H., van den Broeke, M. R., Gardner, A. S., Wouters, B., & van Meijgaard, E. (2013). Irreversible mass loss of Canadian Arctic Archipelago glaciers. *Geophysical Research Letters*, *40*, 1–5. https://doi.org/10.1002/grl.50214

Lenaerts, J. T. M., van den Broeke, M. R., Angelen, J. H., van Meijgaard, E., & Déry, S. J. (2012). Drifting snow climate of the Greenland ice sheet: A study with a regional climate model. *The Cryosphere*, *6*, 891–899. https://doi.org/10.5194/tc-6-891-2012

Millan, R., Mouginot, J., & Rignot, E. (2017). Mass budget of the glaciers and ice caps of the Queen Elizabeth Islands, Canada from 1991 to 2015. *Environmental Research Letters*, *12*(2), 024016. https://doi.org/10.1088/1748-9326/aa5b04

Moholdt, G., Nuth, C., Ove Hagen, J., & Kohler, J. (2010). Recent elevation changes of Svalbard glaciers derived from ICESat laser altimetry. https://doi.org/10.1016/j.rse.2010.06.008

Mortimer, C. A., Sharp, M., & Wouters, B. (2016). Glacier surface temperatures in the Canadian High Arctic, 2000-15. *Journal of Glaciology*, *62*(235), 963–975. https://doi.org/10.1017/jog.2016.80

Munneke Kuipers, P., van den Broeke, M. R., Lenaerts, J. T. M., Flanner, M. G., Gardner, K. A., & van de Berg, W. J. (2011). A new albedo parameterization for use in climate models over the Antarctic ice sheet. *Journal of Geophysical Research*, *116*, D05114. https://doi.org/10.1029/2010JD015113

Noël, B., Fettweis, X., van de Berg, W. J., van den Broeke, M. R., & Erpicum, M. (2014). Sensitivity of Greenland Ice Sheet surface mass balance to perturbations in sea surface temperature and sea ice cover: A study with the regional climate model MAR. *The Cryosphere*, *8*, 1871–1883. https://doi.org/10.5194/tc-8-1871-2014

Noël, B., van de Berg, W. J., Lhermitte, S., Wouters, B., Machguth, H., Howat, I., et al. (2017). A tipping point in refreezing accelerates mass loss of Greenland's glaciers and ice caps. *Nature Communications*, *8*, 14730. https://doi.org/10.1038/ncomms14730

Noël, B., van de Berg, W. J., Machguth, H., Lhermitte, S., Howat, I., Fettweis, X., & van den Broeke, M. R. (2016). A daily, 1 km resolution data set of downscaled Greenland ice sheet surface mass balance (1958-2015). *The Cryosphere*, *10*(5), 2361–2377. https://doi.org/10.5194/tc-10-2361-2016

Noël, B., van de Berg, W. J., van Meijgaard, E., Munneke, P. K., van de Wal, R. S. W., & van den Broeke, M. (2015). Evaluation of the updated regional climate model RACMO2.3: Summer snowfall impact on the Greenland Ice Sheet. *The Cryosphere*, *9*, 1831–1844. https://doi.org/10.5194/tc-9-1831-2015

Overland, J. E., & Wang, M. (2010). Large-scale atmospheric circulation changes are associated with the recent loss of Arctic sea ice. *Tellus*, *62*, 1–9. https://doi.org/10.1111/j.1600-0870.2009.00421.x

Paterson, W. S. B. (Ed.) (1994). *The physics of glaciers* (3rd ed.). United Kingdom, UK: Butterworth Heinemann Oxford.

Pfeffer, W. T., Arendt, A. A., Bliss, A., Bolch, T., Cogley, J. G., Gardner, A. S., et al. (2014). The Randolph glacier inventory: A globally complete inventory of glaciers. *Journal of Glaciology*, *60*(221), 537–552. https://doi.org/10.3189/2014JoG13J176

Polashenski, C. M., Dibb, J. E., Flanner, M. G., Chen, J. Y., Courville, Z. R., Lai, A. M., et al. (2015). Neither dust nor black carbon causing apparent albedo decline in Greenland's dry snow zone Implications for MODIS C5 surface reflectance. *Geophysical Research Letters*, *42*, 9319–9327. https://doi.org/10.1002/2015GL065912

Sharp, M., Burgess, D. O., Cogley, J. G., Ecclestone, M., Labine, C., & Wolken, G. J. (2011a). Extreme melt on Canada's Arctic ice caps in the 21st century. *Geophysical Research Letters*, *38*, L11501. https://doi.org/10.1029/2011GL047381

Sharp, M., Burgess, D. O., Cogley, J. G., Ecclestone, M., Labine, C., & Wolken, G. J. (2011b). Extreme melt on Canada's Arctic ice caps in the 21st century. *Geophysical Research Letters*, *38*, L11501. https://doi.org/10.1029/2011GL047381

Undèn, P., Rontu, L., Järvinen, H., Lynch, P., Calvo, J., Cats, G., et al. (2002). HIRLAM-5, scientific documentation (Tech. Rep.). Norrköping, Sweden: Swedish Meteorological and Hydrological Institute.

Uppala, S. M., Kållberg, P. W., Simmons, A. J., Andrae, U., Bechtold, V. D. C., Fiorino, M., et al. (2005). The ERA-40 re-analysis. *Quarterly Journal of the Royal Meteorological Society*, *131*, 2961–3012.

Van Angelen, J. H., Lenaerts, J. T. M., Lhermitte, S., Fettweis, X., Munneke, P. K., van den Broeke, M. R., et al. (2012). Sensitivity of Greenland Ice Sheet surface mass balance to surface albedo parameterization: A study with a regional climate model. *The Cryosphere*, *6*, 1175–1186. https://doi.org/10.5194/tc-6-1175-2012

Van Meijgaard, E., van Ulft, L. H., van de Berg, W. J., Bosveld, F. C., van den Hurk, B., Lenderink, G., & Siebesma, A. P. (2008). The KNMI regional atmospheric climate model RACMO version 2.1 (Tech. Rep. 302). De Bilt: Royal Netherlands Meteorological Institute.

Van Wychen, W., Copland, L., Burgess, D. O., Gray, L., & Schaffer, N. (2015). Glacier velocities and dynamic discharge from the ice masses of Baffin Island and Bylot Island, Nunavut, Canada. *Canadian Journal of Earth Sciences*, *52*, 980–989. https://doi.org/10.1139/cjes-2015-0087

Van Wychen, W., Davis, J., Burgess, D. O., Copland, L., Gray, L., Sharp, M., & Mortimer, C. (2016). Characterizing interannual variability of glacier dynamics and dynamic discharge (1999-2015) for the ice masses of Ellesmere and Axel Heiberg Islands, Nunavut, Canada. *Journal of Geophysical Research: Earth Surface*, *121*, 39–63. https://doi.org/10.1002/2015JF003708

Vaughan, D. G., Comiso, J. C., Allison, I., Carrasco, J., Kaser, G., Kwok, R., et al. (2013). Observations: Cryosphere. In T. F. Stocker, et al. (Eds.), *Climate change 2013: The physical science basis. Contribution of working group I to the fifth assessment report of the intergovernmental panel on climate change*. Cambridge, UK and New York, USA: Cambridge University Press.

White, P. W. (2001). Part IV: Physical processes (CY23R4) (*Tech. Rep.*): European Centre For Medium-Range Weather Forecasts.

Williamson, S., Sharp, M., Dowdeswell, J., & Benham, T. (2008). Iceberg calving rates from northern Ellesmere Island ice caps, Canadian Arctic, 1999-2003. *Journal of Glaciology*, *54*(186), 391–400. https://doi.org/10.3189/002214308785837048

Wouters, B., Martin-Español, A., Helm, V., Flament, T., van Wessem, J. M., Ligtenberg, S. R. M., et al. (2015). Dynamic thinning of glaciers on the Southern Antarctic Peninsula. *Science*, *348*(6237,) 899–903. https://doi.org/10.1126/science.aaa5727

Zdanowicz, C. M., Fischer, D. A., Clark, I., & Lacelle, D. (2002). An ice-marginal δ^{18}O record from Barnes Ice Cap, Baffin Island, Canada. *Annals of Glaciology*, *35*(1), 145–149. https://doi.org/10.3189/172756402781817031

Zdanowicz, C., Smetny-Sowa, A., Fisher, D., Schaffer, N., Copland, L., Eley, J., & Dupont, F. (2012). Summer melt rates on Penny Ice Cap, Baffin Island: Past and recent trends and implications for regional climate. *Journal of Geophysical Research*, *117*, F02006. https://doi.org/10.1029/2011JF002248